Summer 2018

Crustal structure beneath the eastern margin of the Tibetan Plateau and adjacent areas from receiver function stacking and gravity modeling

Yunxin Peng

Department: Geosciences and Geological and Petroleum Engineering

CRUSTAL STRUCTURE BENEATH THE EASTERN MARGIN OF THE TIBETAN PLATEAU AND ADJACENT AREAS FROM RECEIVER FUNCTION STACKING AND GRAVITY MODELING

by

YUNXIN PENG

A DISSERTATION

Presented to the Faculty of the Graduate School of the

MISSOURI UNIVERSITY OF SCIENCE AND TECHNOLOGY

In Partial Fulfillment of the Requirements for the Degree

DOCTOR OF PHILOSOPHY

in

GEOLOGY AND GEOPHYSICS

2018

Approved
Dr. Kelly H. Liu, Advisor
Dr. Stephen S. Gao, Co-advisor
Dr. David J. Rogers
Dr. Mingzhen Wei
Dr. Youqiang Yu

ABSTRACT

To provide constraints on the mechanisms responsible for the uplift and crustal thickening of the eastern Tibetan Plateau, the thickness and Vp/Vs values of the Moho beneath 153 seismic stations are obtained by stacking P-to-S converted phases from the Moho and gravity modeling. The resulting crustal thickness generally decreases from the northwest to the south-east, from about 60 km in the Bayan Har Block to 30 km in the Sichuan Basin. The crustal Vp/Vs measurements in the Qinling Orogenic Belt, Bayan Har Block, Chuxiong Basin, and Yangtze Platform indicate an overall intermediate to felsic crustal composition. With a relatively thick crust, the inferred crustal Vp/Vs beneath the Bayan Har Block indicates that crustal shortening is accomplished by brittle crustal thickening between rigid crustal blocks, a conclusion that is in line with the observed density structure derived from Bouguer gravity data. High crustal Vp/Vs values up to 1.96 are observed along the Xianshuihe and southern Longmenshan faults. The observed spatial distribution of crustal properties is in agreement with the hypothesis that strain partitioning across deep-rooted faults and the presence of a localized crustal channel flow system both play a vital role in the lateral expansion of the eastern Tibetan Plateau.

ACKNOWLEDGMENTS

I would like to express my gratitude to Dr. Kelly H. Liu and Dr. Stephen S. Gao, for their support, patience, and encouragement throughout my graduate studies. Their technical and editorial advice was essential to the completion of this dissertation and has taught me innumerable lessons and insights on the workings of academic research in general.

My thanks also go to the members of my major committee, Dr. David J. Rogers, Dr. Maochen Ge, Dr. Mingzhen Wei, Dr. Peyman Heidari, and Dr. Youqiang Yu for providing many valuable comments that guided me in my research.

The friendship of colleagues in geology/geophysics group is much appreciated and has led to many interesting and good-spirited discussions relating to this research.

Last, but not least, my deepest gratitude and love for my families' dedication and the many years of support during my studies that provided the foundation for this work.

The Data Management Centre of China National Seismic Network at Institute of Geophysics, China Earthquake Administration (SEISDMC, doi:10.7914/SN/CB) and the IRIS DMC provided the seismic data used in the study. This research is partially funded by the National Key Research and Development Program of China (No. 2016YFC0601005), and by the United States National Science Foundation under grant 0911346.

TABLE OF CONTENTS

Page

LIST OF ILLUSTRATIONS

LIST OF TABLES

NOMENCLATURE

Symbol	Description
H	crustal thickness
Φ	Vp/Vs
σ	Poisson's ratio
RF	receiver function
Longmenshan	LMS

INTRODUCTION

With an average elevation of 4.5 km, the Tibetan Plateau formed as the consequence of the collision between the Indian and Eurasian plates (e.g. Tapponnier et al., 1991). The estimated north-south shortening caused by the collision is at least 1,400 km (Yin and Harrison, 2000), and is accompanied by the thickening, deformation, and extrusion of the crust (e.g. Burchfiel et al., 1995). In spite of numerous studies, the mechanisms responsible for the crustal shortening and uplift remain enigmatic. Among the proposed models, three have drawn the most attention. The first is thickening of the brittle upper crust, in which crustal-scale shortening is accomplished by accumulation of strain mostly localized along the faults (England & Houseman, 1986; Hubbard & Shaw, 2009). The second is the crustal flow model, which advocates the role of mid-lower crustal flow originated from the elevated central part of the plateau (Clark & Royden, 2000). However, whether the flow system pervasively exists beneath all the uplifted area or is limited in localized channels remains enigmatic (e.g. Bai et al., 2010; Li et al., 2015; Xu et al., 2007; Xu et al., 2013). The third model is the whole crustal thickening model, which proposes that the uplift is the product of the combination of localized strain along deep-rooted faults and regional lower crustal rheology (Liu et al., 2014).

The applicability of these models in a given area can be tested by measuring the spatial distribution of crustal properties including the crustal thickness (H) and the ratio between the P and S-wave velocities, Vp/Vs or Φ, which is uniquely related to the Poisson's ratio (σ) by $\sigma = 0.5[1 - 1/(\Phi\ 2 - 1)]$. Laboratory experiments indicated that variations of Vp/Vs are functions of the relative contents of quartz (Vp/Vs =1.49) or plagioclase (Vp/Vs=1.87) (Tarkov & Vavakin, 1982). The global ly averaged Vp/Vs

value for the felsic upper crust is 1.74, and that for the mafic lower crust is 1.81, resulting in an average crustal Vp/Vs of 1.78 (Christensen, 1996). The expected Vp/Vs measurements increase significantly in area with extensive crustal partial melting (Owens & Zandt, 1997). For instance, beneath the Afar Depression, where a transition from continental to oceanic rifting is taking place (Bridges et al., 2010), the observed crustal Vp/Vs value reaches as high as 2.40 (Reed et al., 2014).

While all the aforementioned mechanisms can lead to crustal thickening, the anticipated whole crustal Vp/Vs and density distribution might be different. For the upper crustal thickening model, a lower than normal Vp/Vs is expected due to a greater amount of thickening of the upper crust than the lower crust because the former is felsic and has a lower Vp/Vs than the latter. On the other hand, in areas with the presence of lower crustal flow, elevated Vp/Vs and lower than normal lower crustal density is expected due to partial melting in the lower crust. If crustal thickening is the result of a combination of strain accumulation along major faults and lower crustal flow, the relative role of the two processes can be quantitatively evaluated by the spatial distribution of the Vp/Vs measurements.

1.1. REGIONAL GEOLOGICAL BACKGROUND

The study area is mainly composed of four tectonic domains, including the Qinling Orogenic Belt, Bayan Har Block, Litang Block, and Yangtze Platform (Figure 1.1.).

The Qinling Orogenic Belt represents a zone of continental collision and associated crustal thickening between the Archean-Paleoproterozoic North China and

South China blocks in the Triassic (Yin & Nie, 1993). The Kunlun-Muztagh Suture along the southern margin of the Qinling Belt separates the Qinling Orogenic Belt and the Bayan Har Block (Burchfiel, 1995; Yin & Harrison, 2000).

The Bayan Har and Litang blocks are the eastern-most tectonic units on the Tibetan Plateau, and are highly deformed by the strong compression between the active central Tibetan Plateau to the west and the stable Yangtze Platform to the east. The sinistral Xianshuihe Fault separates the Bayan Har Block to the north and the Litang Block to the south. The basement of the Bayan Har Block was probably a part of the South China Block prior to the late Paleozoic (Burchfiel et al., 1995). The Bayan Har Block can be further divided into the Longmenshan and Ahba blocks by the Longriba Fault (Figure 1.1; Shen et al., 2005; Xu et al., 2008). The Chuxiong intercontinental basin occupies the southern part of the Litang Block (Meng et al., 2009), and is covered by late Permian basalts which are part of the Emeishan Large Igneous Province.

The Yangtze Platform, as a part of the Rodinia supercontinent, has been in a stable state since the late Paleozoic. The Sichuan Basin, suited in the western part of the Yangtze Platform, has three distinguished units divided by the Longquan and Huayingshan faults (Figure 1), including the west plain landform (Chengdu Foreland Basin), the central hilly basin (the western Sichuan Basin), and the east mountain landscape (the eastern Sichuan Basin).

The Longmenshan Fault Zone between the Bayan Har Block and the Sichuan Basin is a thrust-nappe belt. In less than 30 km horizontal distance, the elevation dropped from 5 km to 0.5 km. Given the tectonic significance of the fault and the frequent

occurrence of natural hazards including the 2008 Mw 7.9 Wenchuan earthquake, numerous studies have been conducted over the past several decades in the area.

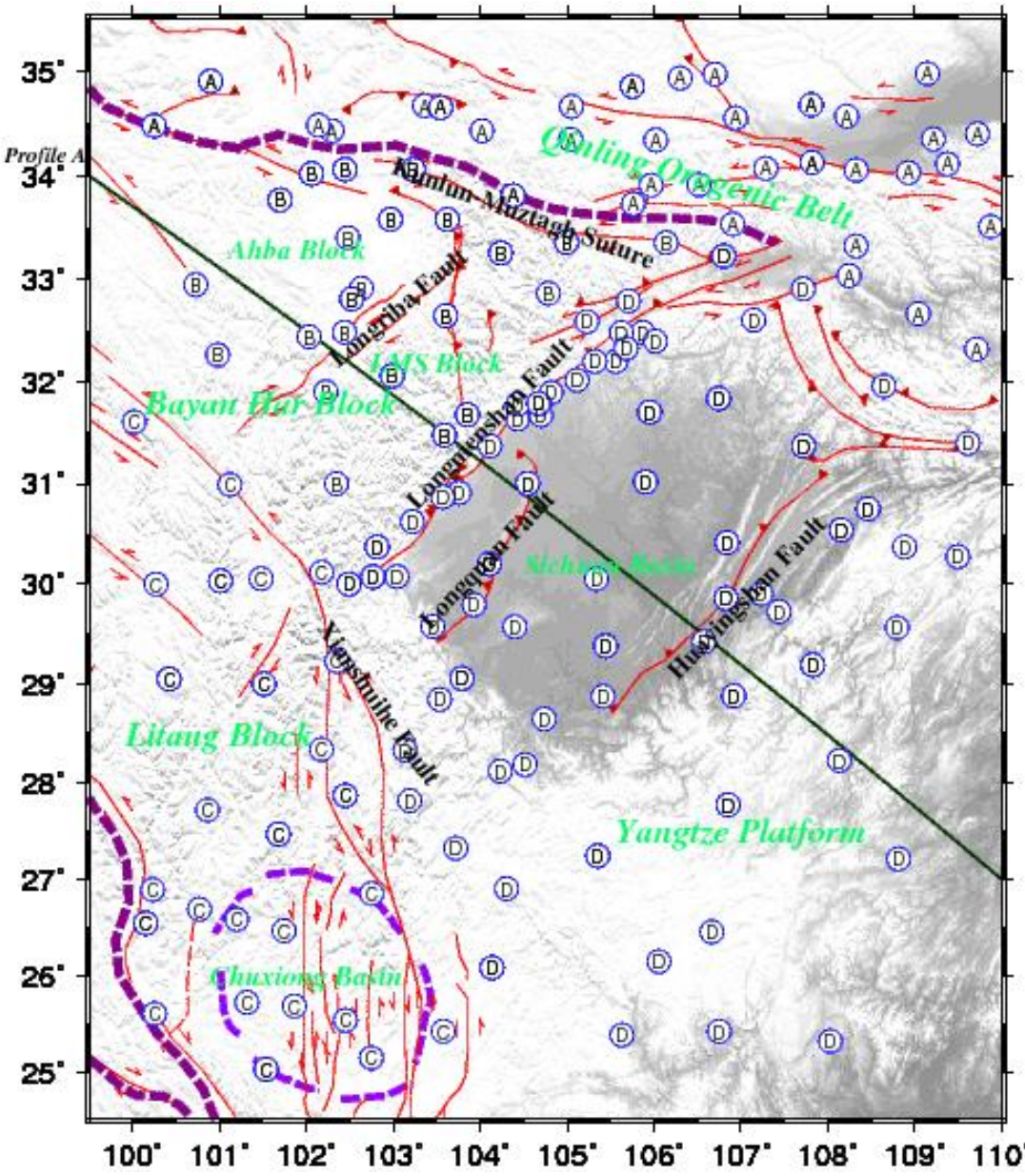

Figure 1.1. A topographic map showing the major tectonic provinces (Xiong et al., 2015; Kong et al., 2016) and distribution of seismic stations used in the study. Circles represent stations with observed P-to-S converted phase from the Moho. A: Qinling Orogenic Belt; B: Bayan Har Block; C: Litang Block; D: Yangtze Platform. Profile A is the locations of the gravity model.

1.2. PREVIOUS CRUSTAL STRUCTURE INVESTIGATIONS

A number of studies have been conducted to estimate the crustal structure beneath the eastern Tibetan Plateau and adjacent areas (Figure 1.2.), mostly by stacking source normalized P-to-S conversions (receiver functions or RFs) from the Moho (He et al., 2014; Li et al., 2015; Liu et al., 2014; Sun et al., 2015; Xu et al., 2007).

1.2.1. Qinling Orogenic Belt. Beneath the Qinling Orogenic Belt, Li et al. (2015) obtained both low (<1.67) and high (>1.87) Vp/Vs measurements, and suggested laterally inhomogeneous crustal structure in this area. In contrast, spatially less varying Vp/Vs values ranging from 1.71 to 1.84 were reported by Liu et al. (2014) for the area.

1.2.2. Bayan Har Block. Observations of crustal Vp/Vs beneath the Bayan Har Block led to different interpretations on the the presence or absence of fluids or felsic materials (Ji et al., 2009; Sun et al., 2015; Wang et al., 2010; Xu et al., 2013). A negative correlation between Moho thickness and Poisson's ratio has been observed and interpreted as the result of upper crust thickening or lower crust delamination (Ji et al., 2009). However, Xu et al. (2013) reported intermediate Vp/Vs (1.71-1.78) in the area and suggested the absence of a mafic lower crust. Wang et al. (2010) interpreted the resulting low Vp/Vs (around 1.76) beneath this area as the evidence of felsic crust. In comparison, a recent study (Sun et al., 2015) argued that the relatively high Vp/Vs (1.74-1.86) observations may indicate the presence of the lower crustal flow. Similarly, Robert et al. (2010) combined migrated receiver functions with gravity data and suggested the absence of a ductile lower crust. In contrast, Lou et al. (2009) compared H − Vp/Vs stacking measurements with Bouguer density anomalies and supported the crustal flow model,

which is also advocated by the low crustal velocities and densities derived from active source seismic data (Wang et al., 2007; Zhang et al., 2014).

1.2.3. Longmenshan Fault Zone. For the LMS Fault Zone, different interpretations have been proposed due to different station distributions. Variable crustal Vp/Vs values ranging from 1.70 to 1.87 have been reported at 9 stations along the LMS Fault Zone (Xu et al., 2013), and an average Vp/Vs of about 1.75 was obtained at 15 stations located in the northern segment of the fault, which suggested an intermediate to felsic crust (Sun et al., 2015). Wang et al. (2010) interpreted the relatively high Vp/Vs (around 1.87) obtained at 9 stations in the southern Longmenshan Fault zone as the consequence of local partial melting. However, Jiang et al. (2012) obtained a detailed density structure in the southern LMS Fault Zone and proposed that the low density anomalies are due to pervasive distribution of crustal fractures.

1.2.4. Litang Block. Despite of some differences, previous studies observed high Vp/Vs values beneath the Litang Block (Li et al., 2016; Wang et al., 2010; Xu et al., 2010). Wang et al. (2010) suggested the presence of localized partial melting in the lower crust on the basis of a high Vp/Vs in the lower crust of about 1.90, which is consistent with the low S-wave velocities observed in the mid-lower crust beneath this area (Li et al., 2016; Liu et al., 2014; Xu et al., 2007). Finally, Li et al. (2016) reported Vp/Vs values at 71 stations ranging from about 1.63 to 1.99, and suggested the existence of two low velocity zones in the mid-lower crust that are probably associated with a channeled flow system.

1.2.5. Sichuan Basin. It is widely accepted by previous studies that the Sichuan Basin is mechanically stronger than the Bayan Har and Litang blocks (e.g. Jiang et al.,

2012; Wang et al., 2007; Zhang et al., 2010). A recent study (Xu et al., 2016) indicated that a crustal stepwise extrusion model is compatible with the elevation in the eastern Tibet, and further pointed out that the similar gravity anomaly between the Chuxiong and Sichuan basins is the evidence of similar composition between these two basins. Xiong et al. (2016) observed a higher density anomaly in the mid-lower crust of the eastern Sichuan Basin relative to that in the western Sichuan Basin, and further suggested lower crustal shortening in the eastern Sichuan Basin.

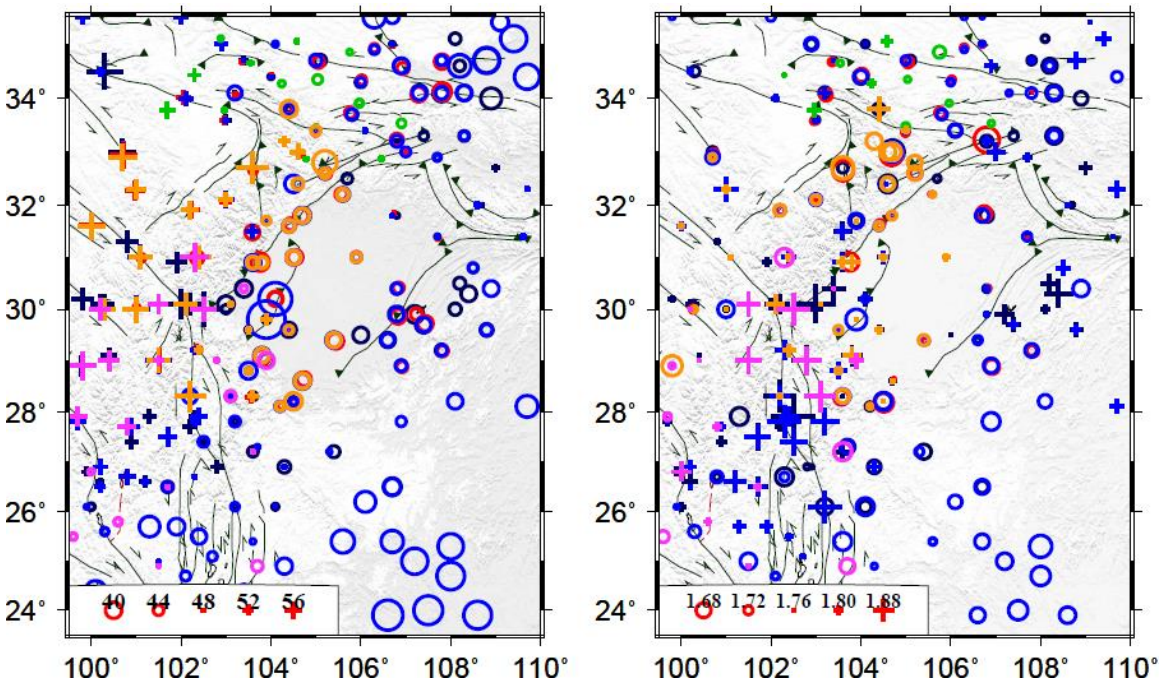

Figure 1.2. Previous receiver function measurements (a) crustal thickness, (b) Vp/Vs. Purple circles and pluses are those from Xu et al. (2007); Black circles and pluses are those from Wang et al. (2010); Blue circles and pluses are those from Xu et al. (2013); Red circles and pluses are those from He et al. (2014); Green circles and pluses are those from Liu et al. (2014); Orange circles and pluses are those from Sun et al. (2015).

1.2.6. Rationale of the Study. This study is motivated by a number of factors, including 1) limited spatial coverage and station density, relative to this study; 2) considerable discrepancies among both the measurements and tectonic interpretation of the measurements for each of the tectonic provinces (Figure 1.2.). The discrepancies in the measurements are caused by the intrinsic nonuniqueness of the H- Φ stacking method that most previous studies used, and by the trade-off between resulting crustal properties and the velocities used. This study uses gravity data as constraints. We also use migrated RFs to provide guidance to the H- Φ observations. 3) more observations have been conducted in the area to provide additional constraints that have not been considered in previous studies on the interpretation of the results.

2. DATA AND METHOD

2.1. DATA

The broadband seismic data set used in the study was obtained from two sources, including the Data Management Center (DMC) of the Incorporated Research Institutions for Seismology (IRIS) for the period of 2003 to 2014 (25 stations), and 2) the Data Management Centre of China National Seismic Network for the time period of 2007 to 2011 (128 stations). All the seismograms with a signal to noise ratio of 4.0 or greater for the first P-wave arrivals on the vertical component from earthquakes in the epicentral distance range of 30◦-180◦ were filtered in the 0.08-0.8 HZ frequency band, and were converted into radial receiver functions (Ammon, 1991; Clayton & Wiggins, 1976). Since terrestrial gravity data are not readily available for this study area, we used the satellite gravity data used to create the 2012 World Gravity Map model (Balmino et al., 2012; Bonvalet et al., 2012). This gravity model was created using gravity data from available land, airborne and marine surveys, and satellite altimetry and long wavelength gravity variations from the Gravity Recovery and Climate Experiment (GRACE) satellite survey. Free-air and spherical Bouguer gravity anomalies were calculated using the WGS84 Geodetic Reference System as a datum. The final Bouguer gravity anomaly data has a spatial resolution of approximately 9 km.

2.2. H – Vp/Vs STACKING OF RECEIVER FUNCTIONS

To obtain the crustal thickness (H) and Vp/Vs, we applied the H − Vp/Vs RF stacking method (Zhu and Kanamori, 2000; Nair et al., 2006) and followed the data processing procedure and parameters detailed in Bashir et al. (2011) and Liu et al. (2017).

The candidate thickness ranges from 35 to 65 km with a step of 0.1 km, and the candidate Vp/Vs ranges from 1.65 to 2.0 in an increment of 0.0025. The weighting factors are 0.5, 0.4, and 0.1 for the Pms, PPms, and PSms phases. Example H − Vp/Vs plots and RFs can be found in Figure 2.1. A crustal P-wave velocity of 6.1 km/s is utilized for moveout correction of the RFs.

2.3. RECEIVER FUNCTION MIGRATION

To demonstrate the quality of the Pms arrivals and provide guidelines for determining the most possible H and Vp/Vs pair on the H − Vp/Vs plot, RFs are migrated along latitude profiles of 2◦ in width. To facilitate ray-tracing, an average crustal S-wave velocity is derived from the assumed P-wave velocity of 6.1 km/s and a constant Vp/Vs of 1.80. The coordinates of the ray-piercing point for each of the RFs are calculated by 1-D ray-tracing at each depth ranging from 0 to 70 km with an interval of 0.1 km. Finally, the amplitudes of RFs with ray-piercing points inside each of the 2◦ (N-S direction) × 0.3◦ (E-W direction) × 0.5 km (vertical direction) blocks are summed.

2.4. GRAVITY MODELING

In order to obtain a more detailed image of the crust, a two and one-half dimensional gravity model was constructed along profile A (Figure 1.1.). Since gravity modeling is nonunique, constraints are necessary in order to obtain a geologically reasonable model. The initial geometries of the model was constrained using results from previous seismic tomography, ambient noise and refraction studies (Wang et al., 2007; Zhang et al., 2011; Zhou et al., 2012), gravity modeling (Wang et al., 2007; Xiong et al., 2016; Xu et al., 2016), geological mapping (Zhao & Cawood, 2012), and the crustal

thicknesses obtained from the H − Vp/Vs stacking in this study. Initial densities were obtained using the P-wave velocities from seismic refraction studies (Wang et al., 2007) converted to densities (Nafe and Drake, 1956), values used in previous gravity modeling (Wang et al., 2007; Xiong et al., 2016; Xu et al., 2016) and Vp/Vs ratios obtained in this study. The initial geometries and densities were then varied by up to 15% in order for the calculated gravity anomalies to match the observed gravity anomalies.

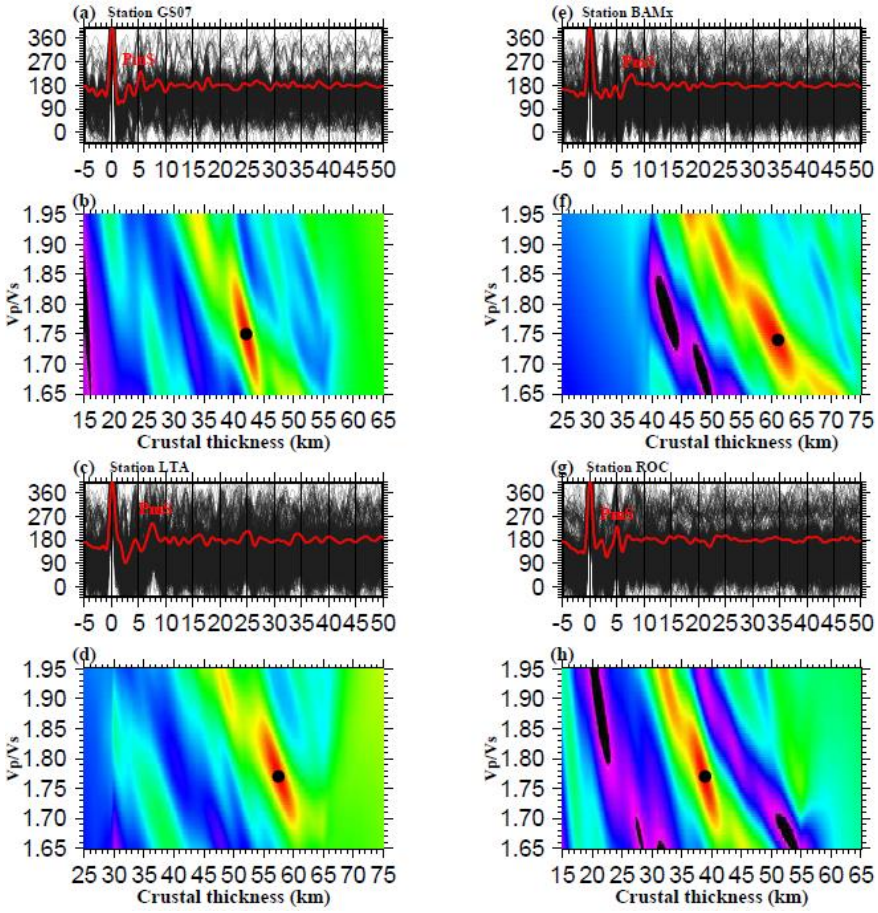

Figure 2.1. Example receiver function analyses for stations located in the Qinling Orogenic Belt, Bayan Har Block, Litang Block, and the Yangtze Platform. (a), (c), (e), and (g) PmS indicates P-to-S converted phases from the Moho; (b), (d), (f), and (h): The dot represents the optimal H and Vp/Vs related to Moho.

3. RESULTS

3.1. RESULTS FROM MIGRATION OF RECEIVER FUNCTION

Robust and spatially continuous Pms arrivals can be observed on E-W the profiles of migrated RFs (Figure 3.1.). Although the migration was performed using a fixed Vp/Vs of 1.80, the Moho depths from the H − Vp/Vs stacking (Figure 3.2.) are mostly comparable to the depth of the maximum stacking amplitude on the RF profiles (Figure 3.1.). In general, a trend of eastward shallowing of the Moho is observed on five profiles. The trend is gentle along the southernmost two profiles (Figures 3.1a. and 3.1b.) which traverse the Litang Block and part of the Yangtze Platform south of the Sichuan Basin. Further north, the profile sampling the northern Litang Block and the southern Sichuan Basin (Figure 3.1c.) shows more dramatic variations of the Moho depth, from about 60 km beneath the Litang Block to about 40 km beneath the Sichuan Basin over a distance of about 300 km. Similar Moho undulations are found along the two profiles traversing the Bayan Har Block and the Sichuan Basin (Figures 3.1d. and 3.1e.), but with a smaller gradient mostly due to the thicker crust beneath the Bayan Har Block. The smallest gradient is found along the northernmost profile which mostly samples the Qinling Belt (Figure 3.1f.).

3.2. CRUSTAL THICKNESS AND Vp/Vs RATIO

The resulting crustal thickness in the study area ranges from 32.1 km to 61.0 km with an average of 45.3 ±6.1 km, and the Vp/Vs ranges from 1.67 to 1.96 with a mean of 1.79 ±0.06 (Figures 3.2. and 3.3.). Measurements from this study show a generally

consistency with previous studies at common stations (Figure 3.4.). For some stations, previous studies only observed crustal thickness (Liu et al., 2014), or the results are not compatible with the geology in the area. (e.g. Station JYA in the Sichuan Basin with a resulting crustal thickness of 25.6 km and Vp/Vs of 1.64 from Xu et al., (2014). What's more, previous studies have some disagreements with each other. For station QLIT, which located in the eastern Qinling Orogenic Belt, the resulting thickness and Vp/Vs from this study are 33.5 ±0.2 km and 1.79 ±0.01, respectively, shows a consistency with Xu et al., (2013) (35.7 ±1.5 km and 1.72 ±0.05, respectively), and disagreement with Wang et al., (2010) (41.5 km and 1.84, respectively). For station YGDx, which situated in the Longquan Fault, the resulting thickness and Vp/Vs from this study is 40.1 ±0.1 km and 1.89 ±0.003, respectively, which is similar to those from Wang et al., (2010) (41.5 km and 1.84), and inconsistent with Xu et al., (2013) (28.8 ±1.9 km and 1.73 ±0.06) and Sun et al., (2015) (49 km and no observation of Vp/Vs value). With a significantly improved spatial coverage in the study area, our results provide more information on crustal structure beneath the eastern Tibetan Plateau and adjacent areas.

3.2.1. Qinling Orogenic Belt. The Qinling Orogenic Belt is sampled by 34 stations. This area is characterized by crustal thicknesses ranging from 32.4 km to 58.0 km with a mean of 43.2 ±6.2 km and crustal Vp/Vs ranging from 1.71 to 1.90 with a mean of 1.78 ±0.04. The crust thins gradually toward the east, while no corresponding spatial variation in the Vp/Vs observations is found.

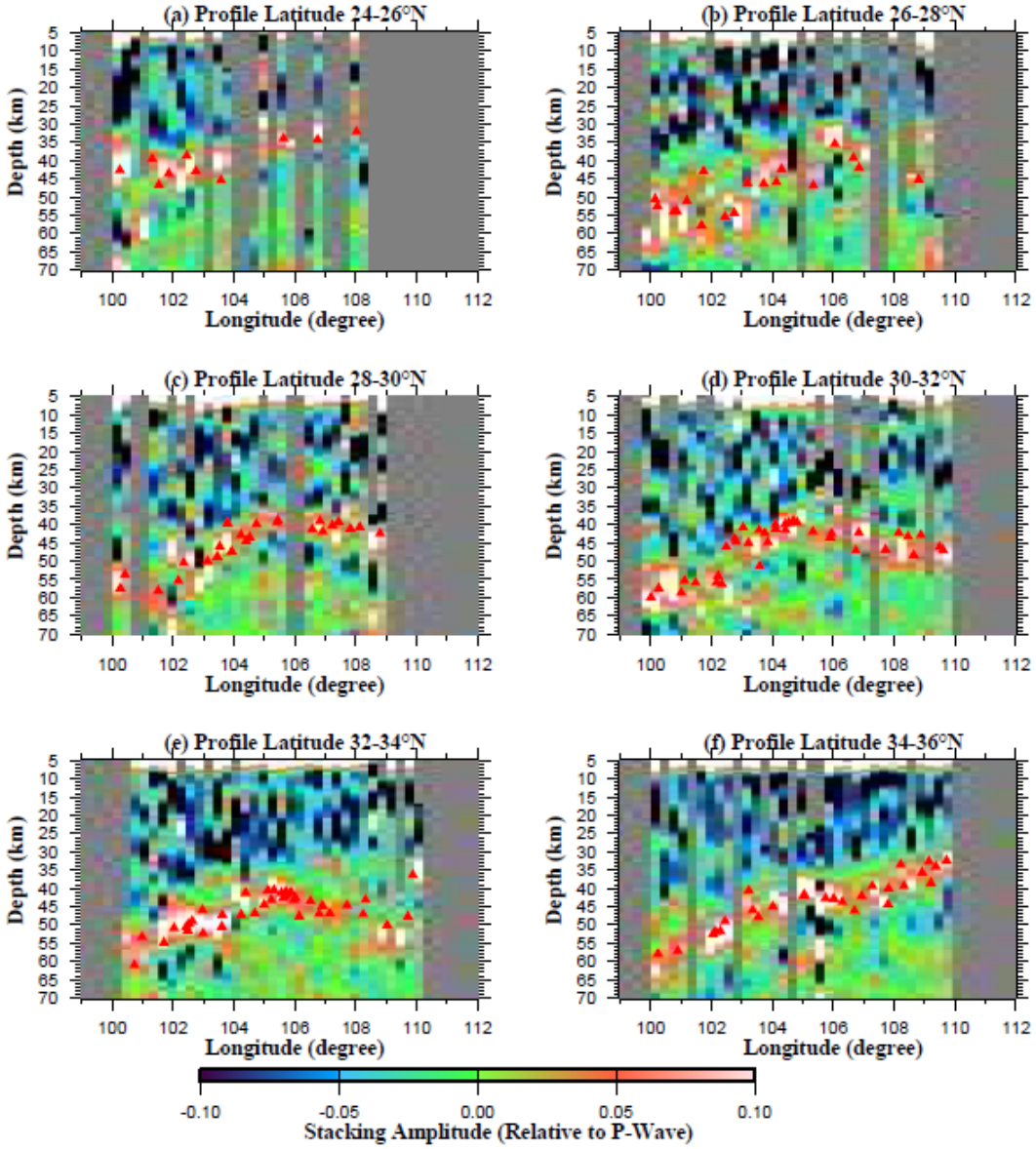

Figure 3.1. Depth series from stacking of RFs in 2◦ wide E-W band along six latitude profiles. The triangles indicate the crustal thickness derived from H−Vp/Vs method which correspond with the highest stacking amplitude along the profiles.

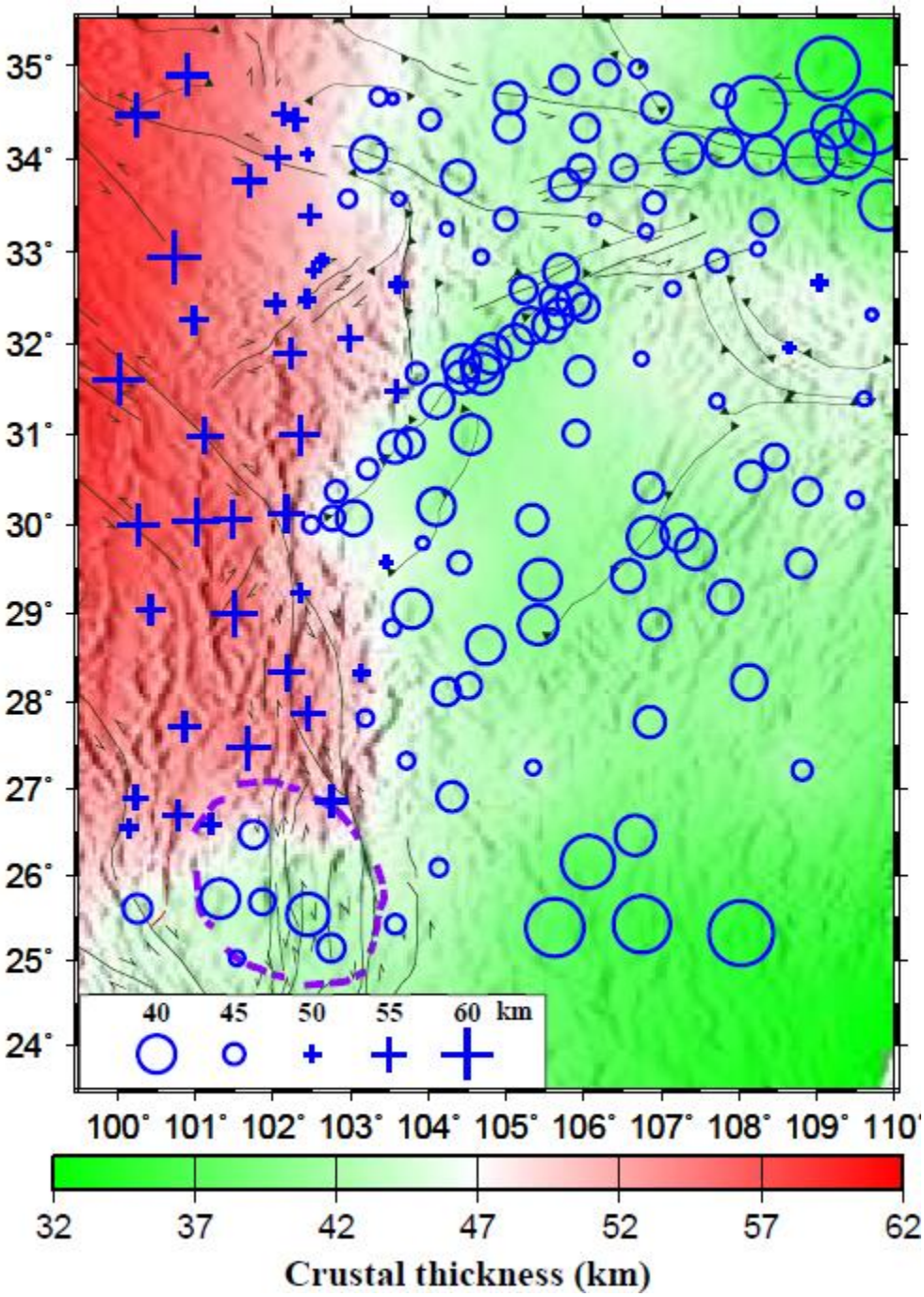

Figure 3.2. Observed crustal thickness plotted on top of smoothed crustal thickness measurements. The legend indicates a relatively larger values in pluses and relatively smaller values in circles.

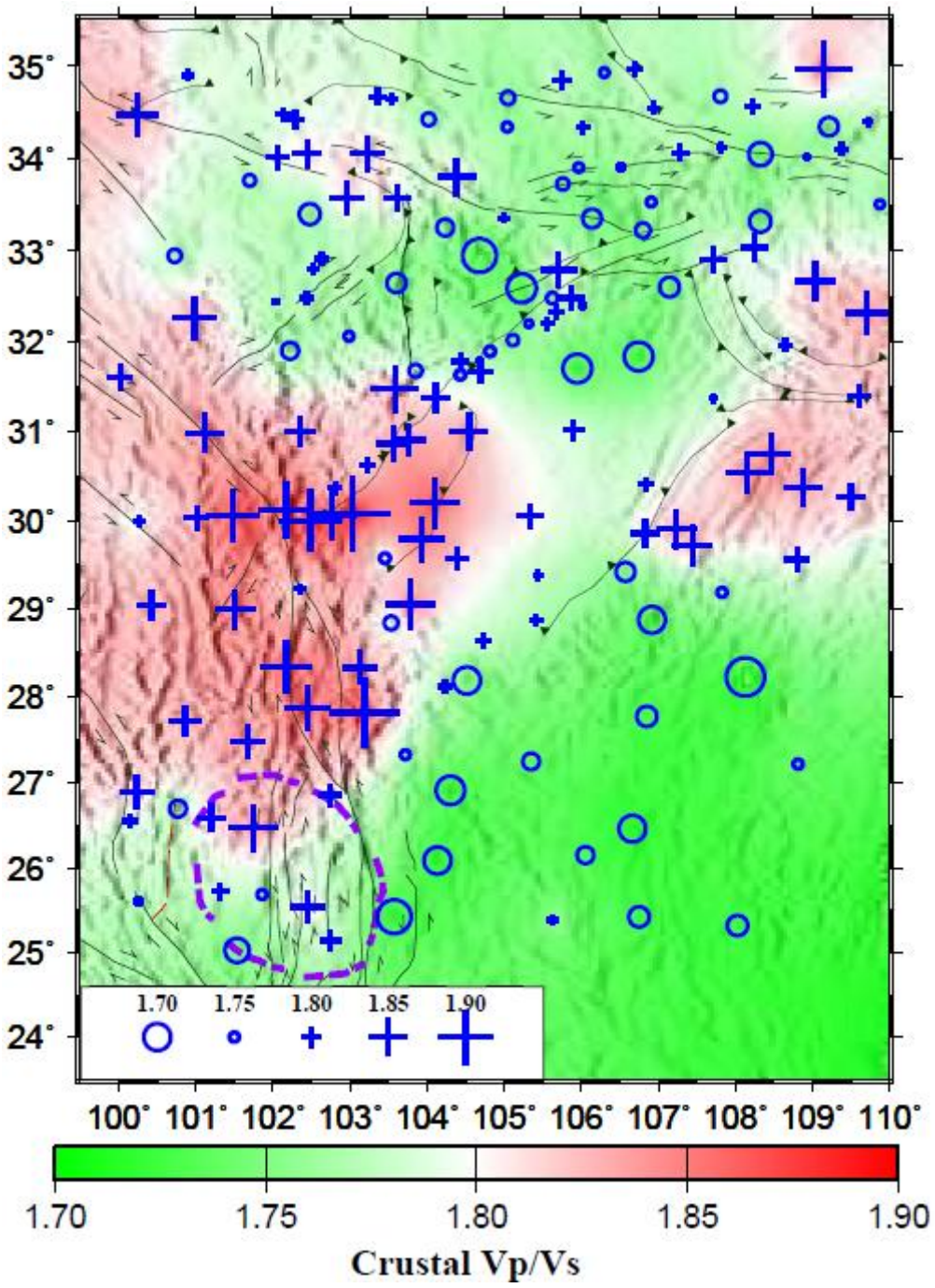

Figure 3.3. Observed crustal Vp/Vs plotted on top of smoothed crustal Vp/Vs measurements. The legend indicates a relatively larger values in pluses and relatively smaller values in circles.

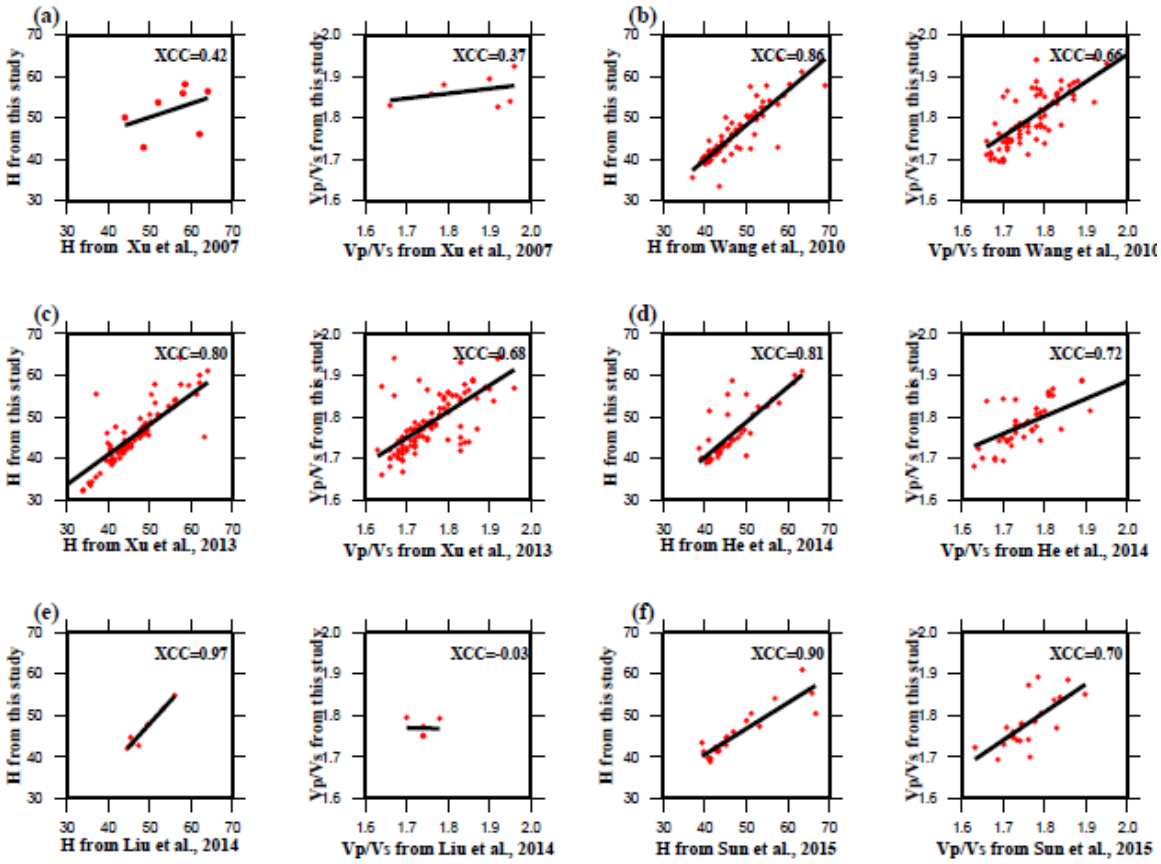

Figure 3.4. Comparison of H (left panels) and Vp/Vs (right panels) measurements obtained from this study (horizontal axis) with those from previous studies (vertical axis) at common stations. (a) Xu et al., 2007; (b) Wang et al., 2010; (c) Xu et al., 2013; (d) He et al., 2014; (e) Liu et al., 2014; (f) Sun et al., 2015.

3.2.2. Bayan Har Block. The measured crustal thicknesses in the Bayan Har Block observed at 23 stations range from 40.6 km to 61.0 km with a mean of 50.9 ±4.4 km, and the Vp/Vs values range from 1.68 to 1.88 with a mean of 1.78 ±0.05. One of the interesting observations is that the H values have an E-W gradient and is significantly different from the NE-SW strike of the LMS Fault zone, which is the boundary of the Tibetan Plateau in this area (Figure 3.2.). The area along the boundary between the Bayan

Har and Litang blocks, which is the Xianshuihe Fault, possesses higher than normal Vp/Vs values of around 1.85. Another interesting feature is that the Vp/Vs measurements observed in the southern half of the LMS Fault zone are about 1.88 which are significantly higher than those observed in the northern half of the fault zone (Figure 3.3.). The largest Vp/Vs in the entire study area is found at the southern end of the LMS Fault zone.

3.2.3. Litang Block. In the Litang Block, sharp contrasts in both the observed H and Vp/Vs values are found between the Chuxiong Basin and the rest of the Block. The crustal thickness in the latter is about 55 km which is about 15 km greater than that observed at stations in the former (Figure 3.2.). Similarly, relative to the Chuxiong Basin, significantly greater Vp/Vs values are observed in the area of the Litang Block north of the Chuxiong Basin (Figure 3.3.).

3.2.4. Yangtze Platform. The mean crustal thickness and Vp/Vs measured at 70 stations on the Yangtze Platform is 42.4 ±3.5 km and 1.79 ±0.07, respectively, and both are comparable to values obtained at typical cratonic areas such as central North America (e.g., Figures 5. and 6 in Liu et al., 2017). The H values range from 32.11 to 50.1 km and show a less significant spatial variation than the other three areas. Large Vp/Vs values are found in the area the east of the Huayingshan Fault in the northeastern part of the Sichuan Basin, as well as the southwestern part of the basin adjacent to the southern segment of the LMS Fault zone.

Table 3.1. Observations of crustal thickness (H) and Vp/Vs (Φ).

Area	Numbers of stations	H(km) range	mean H(km)	ϕ range	mean ϕ
A	34	32.37-57.95	43.16± 1.06	1.711-1.903	1.779± 0.008
B	23	40.61-61.03	50.09± 0.92	1.68-1.878	1.776± 0.011
C	26	38.65-60.0	51.28± 1.25	1.68-1.904	1.813± 0.011
D	70	32.11-50.1	42.43± 0.42	1.667-1.963	1.786± 0.008

3.3. GRAVITY MODELING

The resultant gravity model (Figure 3.5.) which in general agrees with the crustal thicknesses determined from the H-k stacking of receiver functions (Figure 3.2.). The main portions of the model are the upper, middle and lower crust, the upper mantle, metamorphic lithologies of the Yangtze Craton (density-2.75 gm/cc), Mesozoic and Paleozoic sequences of the Sichuan Basin (density-2.45 gm/cc) and thinner sedimentary cover over the Bayan Har Block and the Yangtze Platform (density-2.50 gm/cc). The crust is thicker under the Bayan Har Block (maximum of 53 km) and abrupt thins at the Longmenshan Fault to roughly 44 km under the Sichuan Basin and Yangtze Platform. Additionally the densities vary of the middle, lower and upper mantle varies northwest and southeast of the Longmenshan Fault with consistently higher values under the Sichuan Basin and Yangtze Platform. This agrees with the Vp/Vs ratios (Figure 3.3.) where higher Vp/Vs ratios are found under the Sichuan Basin and Yangtze Platform and are interpreted to represent intermediate to mafic material in the crust. The resultant densities of the middle and lower crust (2.80 and 2.98 gm/cc) under the Bayan Har Block suggest that these regions are more intermediate in composition than the southeastern portions of the model. Modeling of the gravity data when constrained by the crustal thicknesses (Figure 3.2.) required higher densities in the crustal /or upper mantle layers

southeast of the Longmenshan Fault. However, modeling could not determine in which layer required the density increase and using densities with higher contrasts than shown in Figure 3.5. resulted in a greater misfit to the observed Bouguer gravity anomalies. Additionally by putting the density variation into one layer (e.g., lower crust) and keeping the same densities in the other crustal and upper mantle bodies required a density variation that was deemed too high based on the variation of the Vp/Vs ratios. The thinner crust under the Yangtze Platform and Craton agrees with previous studies (Li et al., 2015) who suggested that the Yangtze Craton has lost is crust root during the rollback of the Paleo-Pacific subducting plate. Thus, the final model represents one representation of the crustal structure that fits all available constraints.

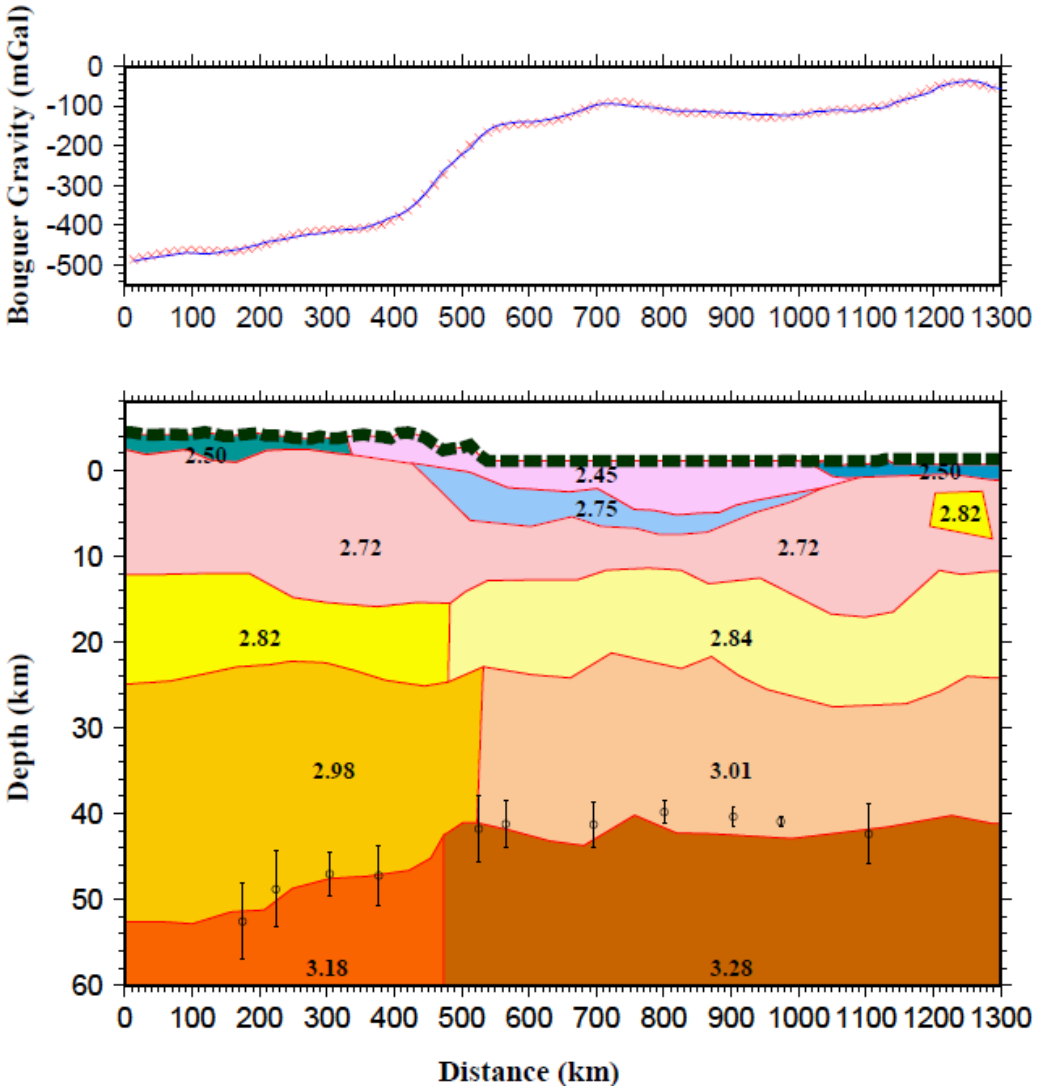

Figure 3.5. Gravity model along Profile A (Figure 1.1.) with 200 km wide band. Red crosses represent observed gravity anomalies. Blue line represents calculated gravity anomalies. Dots represent resulting H−Vp/Vs measurements from this study. Densities are in gm/cc.

4. DISCUSSIONS

4.1. FELSIC TO INTERMEDIATE CRUST IN THE QINLING OROGENIC BELT

The resulting crustal thickness in the Qinling Orogenic Belt decreases from west to east (Figure 3.3.). One of the previously proposed models (Clark & Royden, 2000; Royden et al., 2008) attributes the thickening to thickening of the lower crust through a lower crustal flow system. Because the lower crust has higher Vp/Vs than the upper crust, this model predicts an eastward decrease in the overall crustal Vp/Vs along the Qinling Orogenic Belt. Such a decrease is not observed. Instead, the observations of the denser crust beneath the Qinling Orogenic Belt is the product of the Cenozoic uplift of the simultaneous thickening of the upper and lower crust associated with the India-Eurasia collision.

4.2. CRUSTAL DEFORMATION IN THE BAYAN HAR BLOCK

With a relatively thick crust, the resulting crustal Vp/Vs in the Bayan Har Block is low, which is consistent with previous studies (Ji et al., 2009; Wang et al., 2010; Xu et al., 2013; He et al., 2014; Li et al., 2015), indicating a dominantly intermediate lower crust (Christensen, 1996) (Figure 3.3.). The lack of a mafic lower crust with high P-wave velocity in this area is also suggested by other studies (Wang et al., 2013). With the continuous intensive compressional stress from the central Tibet and the blockage from rigid Sichuan Basin, the apparent crustal structure of the Bayan Har Block is the result of brittle upper crustal deformation (Tapponnier et al., 2001). GPS measurements have found that the Longriba Fault, as a velocity gradient belt, separates two areas with

different tectonic activities (Shen et al., 2005; Xu et al., 2007). A recent study further indicates that a large-scale crustal reworking happened in the area between the LMS Fault and the Longriba Fault (Guo et al., 2015).

4.3. CONSTRAINTS ON CRUSTAL RHEOLOGY AND LOCALIZATION STRAIN ALONG THE XIANSHUIHE FAULT

The presence of partial melting in the crust would increase the crustal Vp/Vs because of a greater decrease of crustal Vs than Vp when partial melt is present (Budiansky & O'Connell., 1976). The high Vp/Vs observed along the Xianshuihe Fault suggests the presence of regional partial melting, a conclusion that is consistent with previous RF studies (Xu et al., 2007; Wang et al., 2010; Xu et al., 2013). The existence of a lower crustal flow system has also been proposed based on observations of high electrical conductivity (Bai et al., 2010), significant crustal seismic anisotropy (Sun et al., 2015; Kong et al., 2016), and low shear wave speed (Xu et al., 2007; Liu et al., 2014; Li et al., 2016).

In addition, as the transition zone of the mechanically contrast between relatively weak the overall plateau and relatively rigid Yangtze Platform, the lateral extrusion of the interaction of the crustal blocks would facilitate regional strain release (Gan et al., 2007; Hubbard & Shaw, 2009). The effect of crustal rheology further weakened the region, leading to the strain accumulation along the deep-rooted faults.

As the interrelated and interact between the localization of strain along the major faults and regional crustal flow, the crustal deformation is accomplished (Liu et al.,2014).

4.4. POSSIBLE BLOCKAGE OF LOWER CRUSTAL FLOW BY THE CHUXIONG BASIN

The northern part of the Litang Block is characterized by a thick crust with larger than normal Vp/Vs observations (Figures 3.2. and 3.3.), suggesting the presence of lower crustal thickening probably through southward flow of lower crustal materials. In contrast to the northern part of the Litang Block, the Chuxiong Basin situated in the southern Litang Block is characterized by significantly decreased crustal thickness and Vp/Vs, suggesting intermediate to felsic crustal composition which excludes the possibilities of lower crustal partial melting.

This is consistent with the observations from magnetotelluric (Bai et al., 2010) and surface wave tomography (Li et al., 2016) studies. In addition, previous gravity anomaly study and geological investigation indicated a similar crustal composition of the Sichuan and Chuxiong basins, and suggested that the Chuxiong Basin was a part of the Yangtze Platform before the Himalayan orogeny building (Wang et al., 2014; Xiong et al., 2016). Therefore, our observations are consistent with the model that the southward crustal flow is blocked by the rigid Chuxiong Basin.

4.5. DIFFERENT CRUSTAL STRUCTURE BETWEEN THE WEST AND EAST SICHUAN BASIN

The western Sichuan Basin shows relatively low Vp/Vs relative to the global average while the eastern Sichuan Basin shows a more mafic crust (Figure 3.3.). This is in agreement with the recent observation that the western and eastern Sichuan Basin belong to two different continental nucleuses (Wu et al., 2012).

4.6. LATERAL VARIATION OF CRUSTAL PROPERTIES ALONG THE LMS FAULT AND ITS RELATIONSHIP WITH EARTHQUAKE DISTRIBUTION

Different crustal Vp/Vs between the southern and northern LMS Fault are observed. The relatively low Vp/Vs values in the northern segment indicate a more felsic composition which is consistent with previous studies (Wang et al., 2010; Wang et al., 2011; Xu et al., 2013; He et al., 2014). The significantly high crustal Vp/Vs along the southern LMS Fault suggests the presence of partial melt (Owens & Zandt, 1997; Lei et al., 2007; Wang et al., 2010). Previous studies indicated that partial melting in the deep crust does not necessarily require an ancient overthickened crust or crustal delamination (Qian et al., 2013). Combined with low resistivity (Zhao et al., 2015) and low Vp and Vs (Lei et al., 2009; Wang et al., 2011), the observed relatively high Vp/Vs of the southern LMS Fault further indicated the existence of fluid in the lower crust. A ductile lower crust beneath the southern LMS Fault is also observed by a recent seismic reflection study (Feng et al., 2016). The ductile lower crust fits well with the massive energy accumulated in the LMS Fault with a low surface GPS rate (Shen et al., 2005; Wang et al., 2011). The accumulation and transfer of fluid beneath the southern LMS Fault may provide adequate energy for facilitating regional tectonic activities and lead to great earthquakes such as the 2008 Mw 7.9 Wenchuan earthquake.

5. CONCLUSIONS

We obtained the crustal structure in the eastern Tibetan Plateau and adjacent areas from teleseismic receiver functions and gravity data modeling. Several conclusions can be drawn from the observations:

1) Intermediate crust is observed in the Bayan Har Block and Qinling Orogenic Belt, indicating a lack of mafic layer and supporting a simultaneous whole crustal thickening model.

2) Resulting ultra-high crustal Vp/Vs beneath the the northern part of the Litang Block Block supports the presence of lower crustal flow, which is probably blocked by the strong crust beneath the Chuxiong Basin in which normal crustal thickness and Vp/Vs are observed.

3) The crust of the eastern Sichuan Basin is more mafic than that of the western Sichuan Basin, suggesting a different crustal structure between the two sides of the Sichuan Basin.

4) The ductile lower crustal layer in the southern LMS Fault could play a vital role in triggering large regional earthquakes.

APPENDIX A.

EXAMPLE RECEIVER FUNCTION ANALYSES

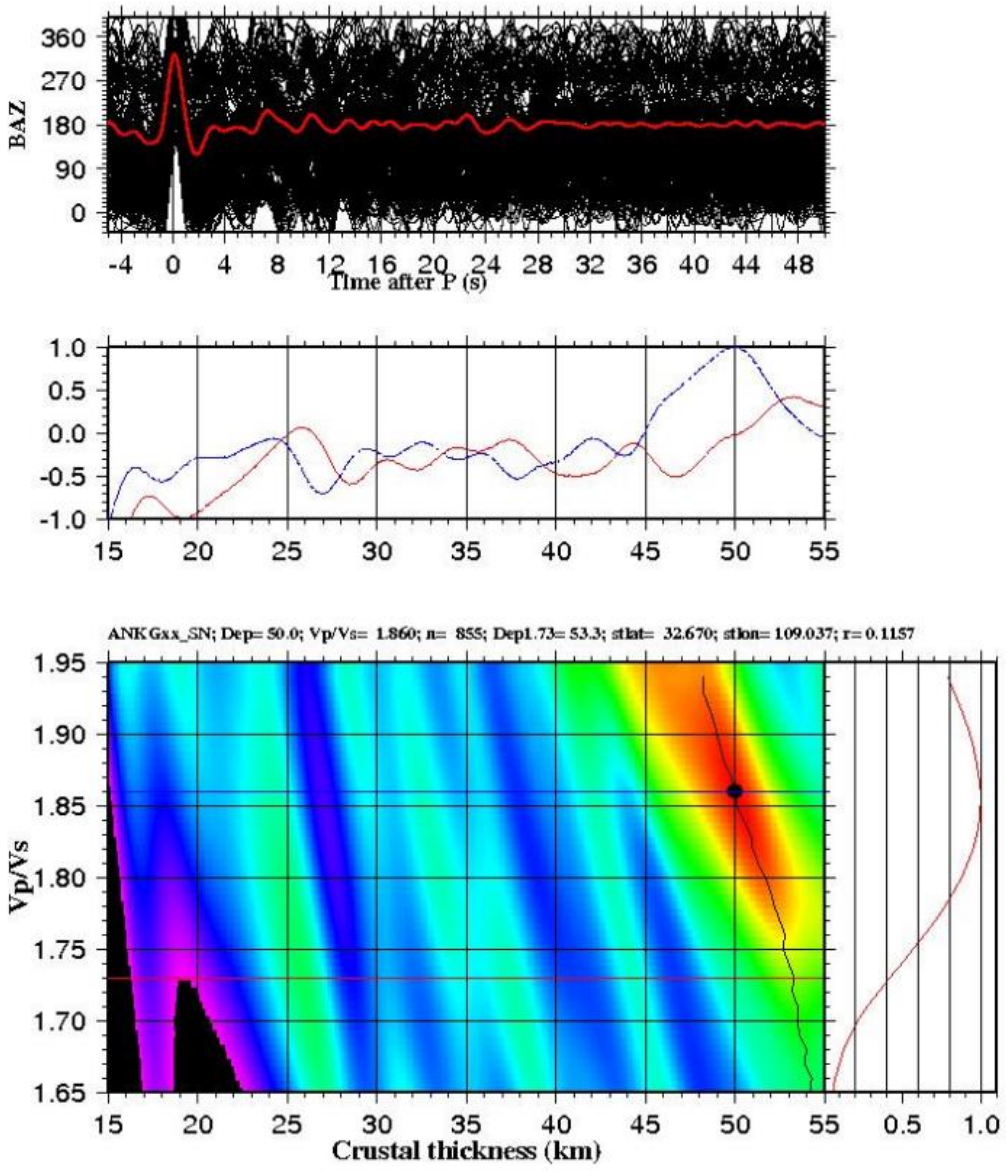

Figure S1. Example receiver function analyses for station ANKGxx_SN located in the Qinling Orogenic Belt. The dot represents the optimal H and Vp/Vs related to Moho.

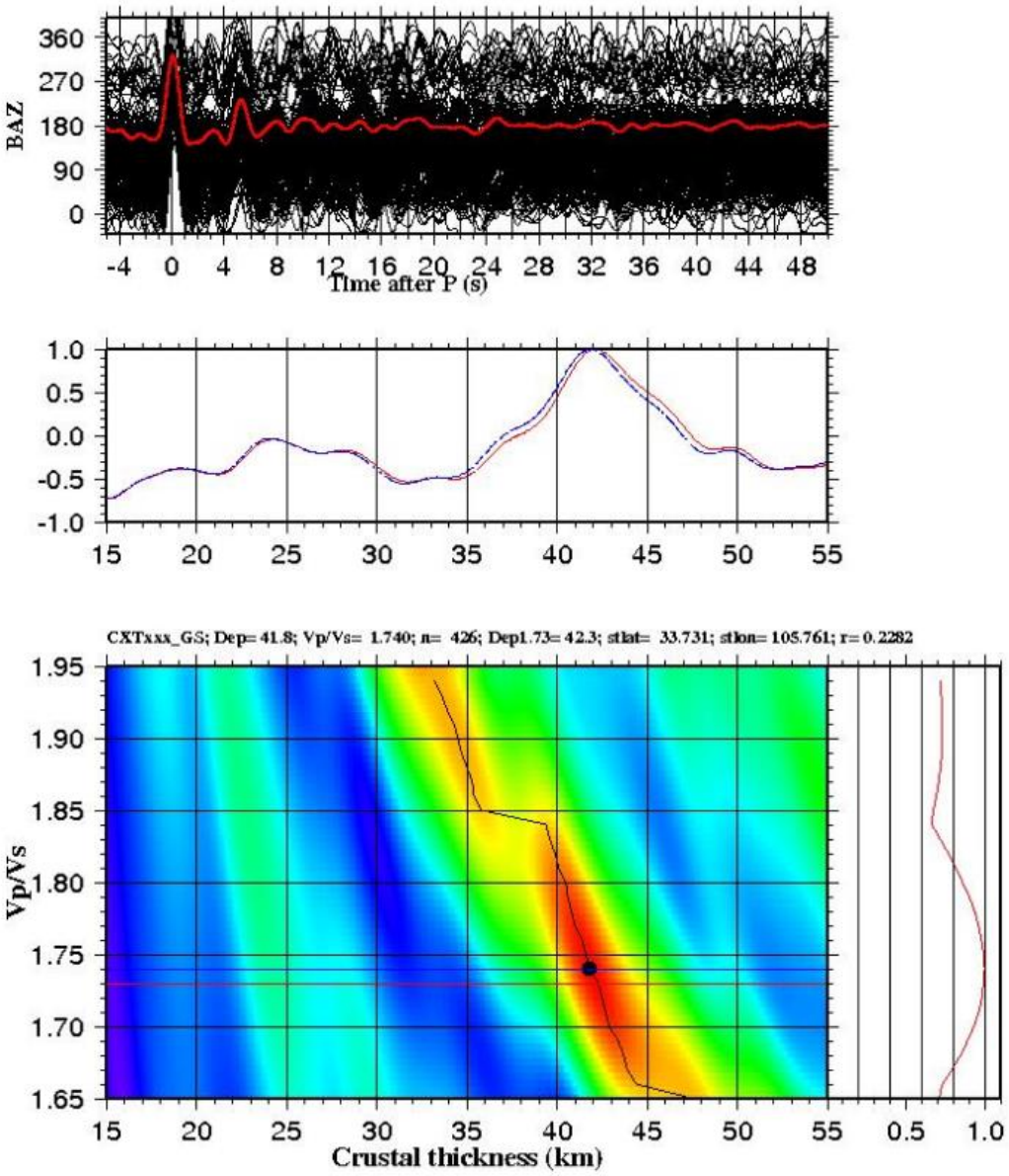

Figure S2. Example receiver function analyses for station CXTxxx_GS located in the Qinling Orogenic Belt. The dot represents the optimal H and Vp/Vs related to Moho.

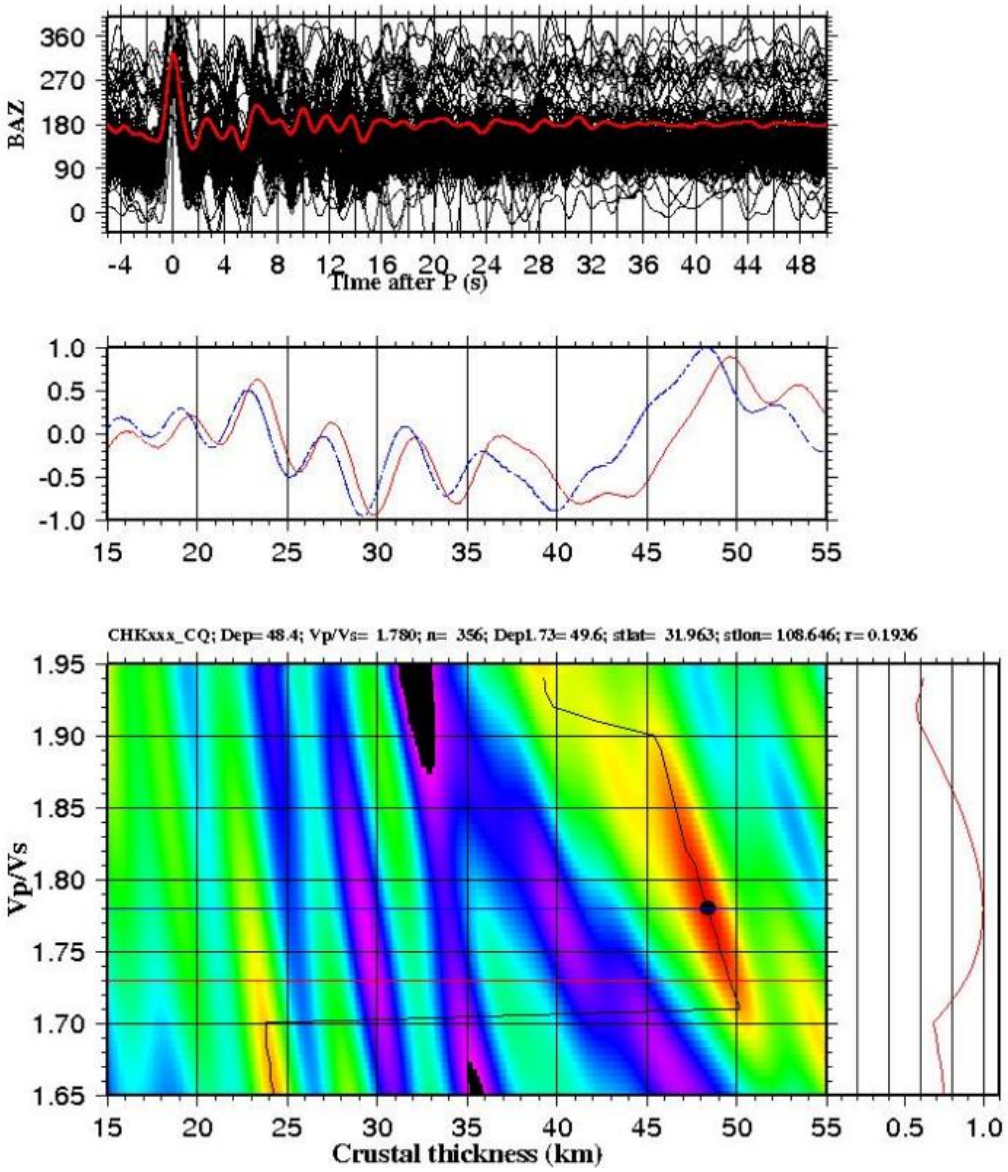

Figure S3. Example receiver function analyses for station CHKxxx_CQ located in the Bayan Har Block. The dot represents the optimal H and Vp/Vs related to Moho.

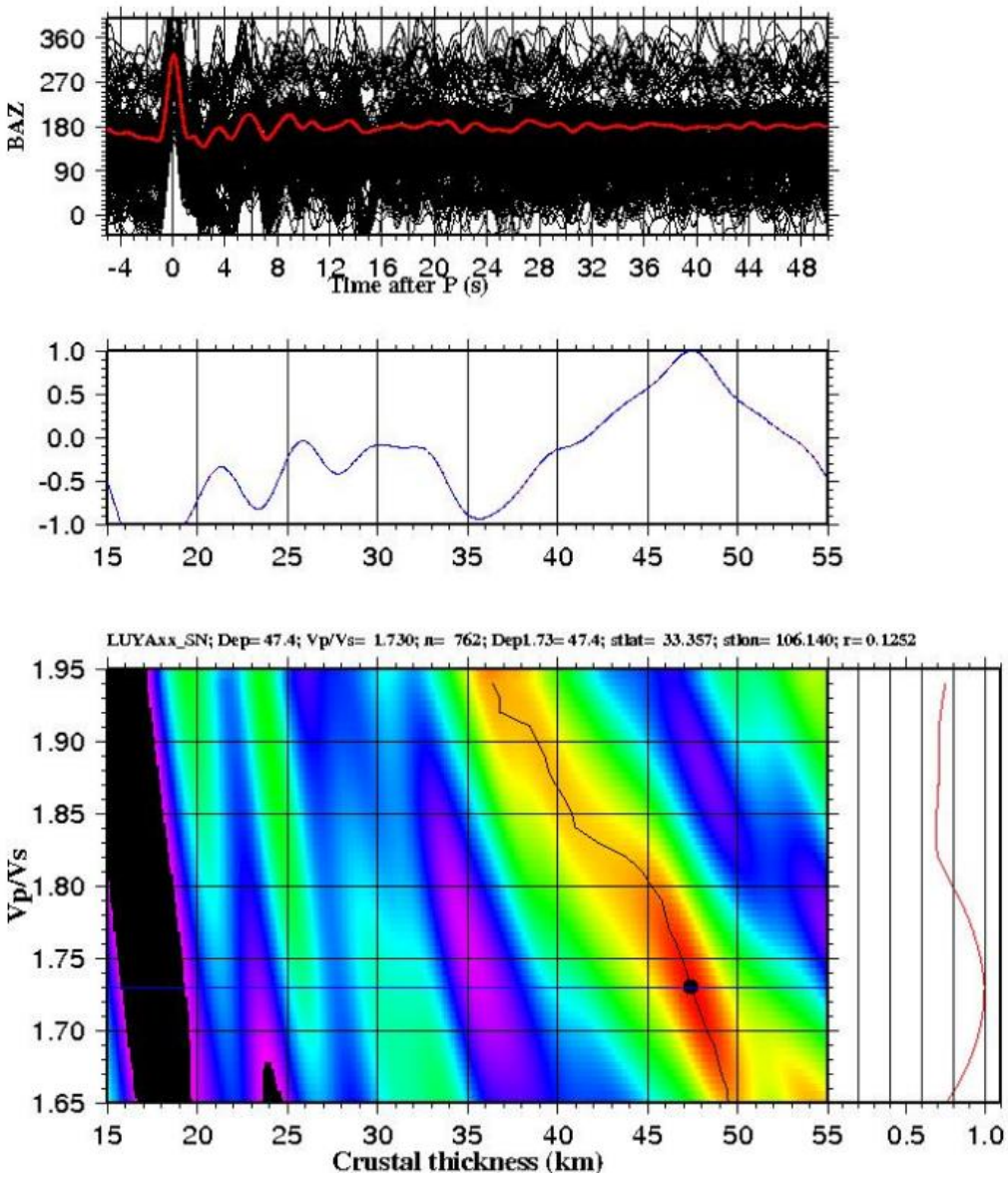

Figure S4. Example receiver function analyses for station LUYAxx_SN located in the Bayan Har Block. The dot represents the optimal H and Vp/Vs related to Moho.

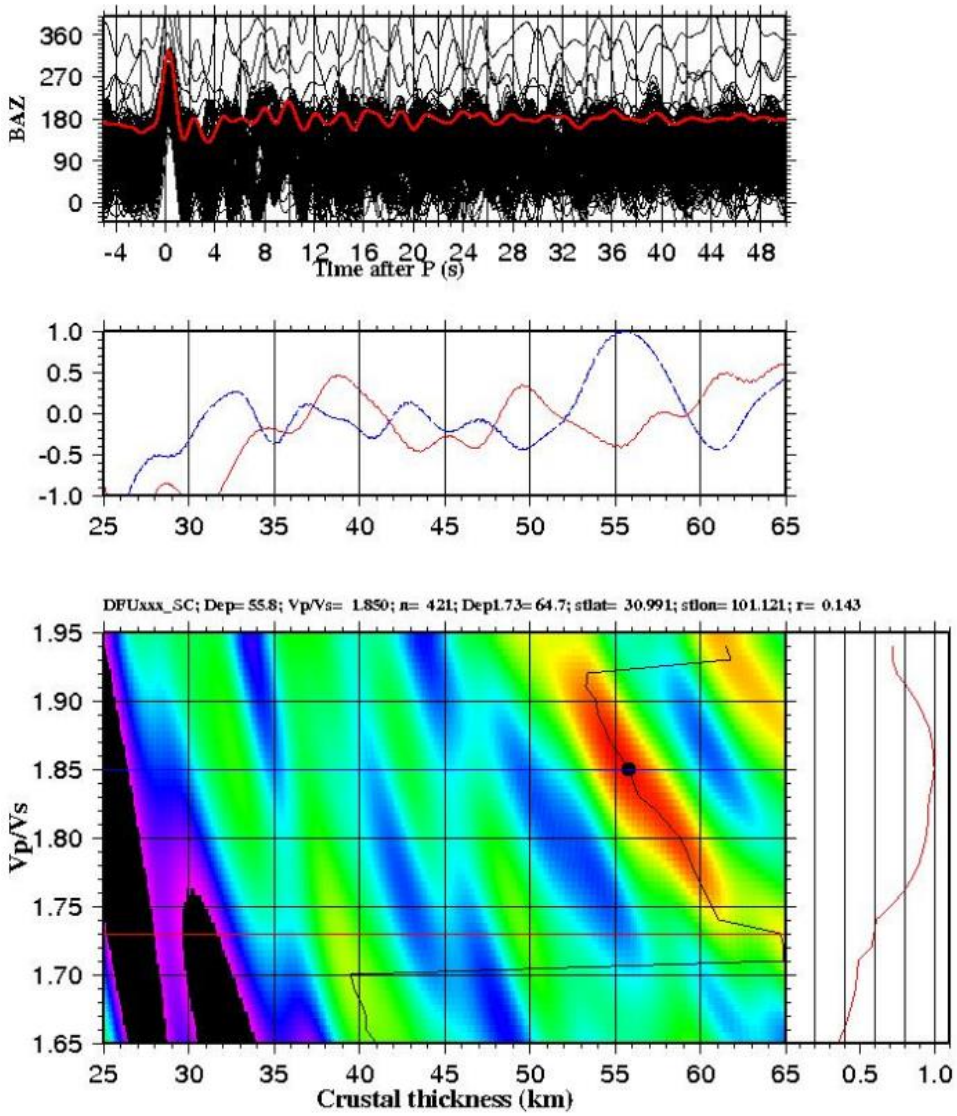

Figure S5. Example receiver function analyses for station DFUxxx_SC located in the Litang Block. The dot represents the optimal H and Vp/Vs related to Moho.

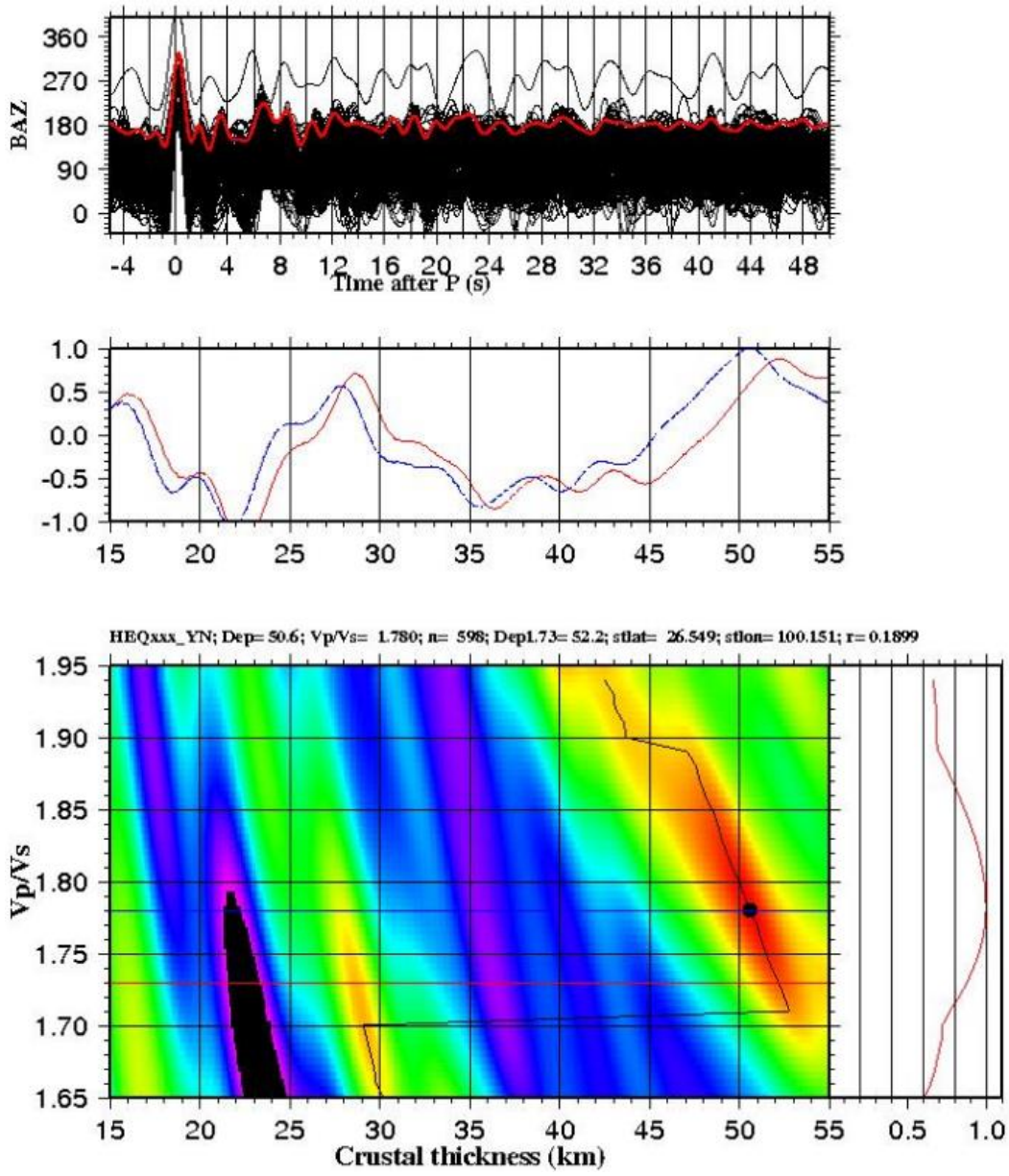

Figure S6. Example receiver function analyses for stationHEQxxx_YN located in the Litang Block.The dot represents the optimal H and Vp/Vs related to Moho.

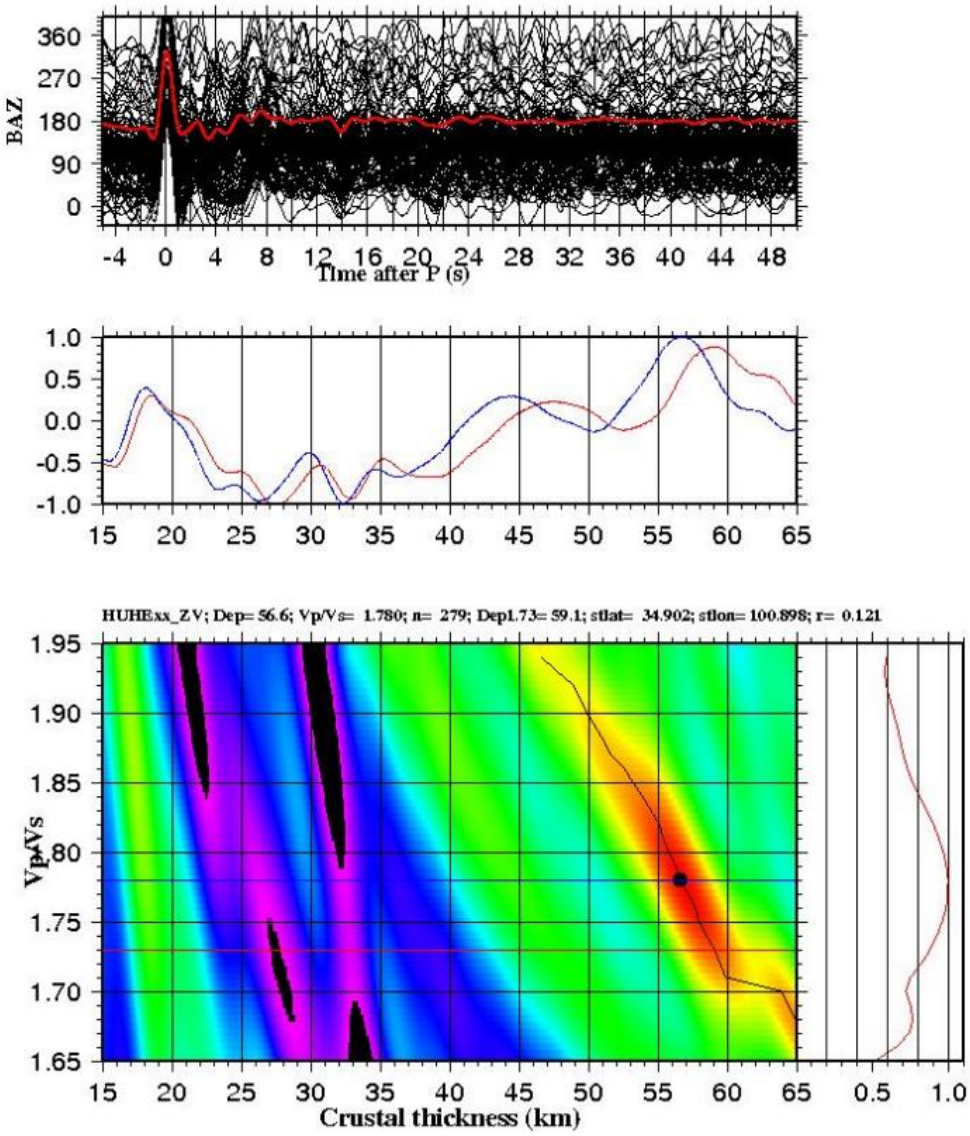

Figure S7. Example receiver function analyses for station HUHExx_ZV located in the Yangtze Platform. The dot represents the optimal H and Vp/Vs related to Moho.

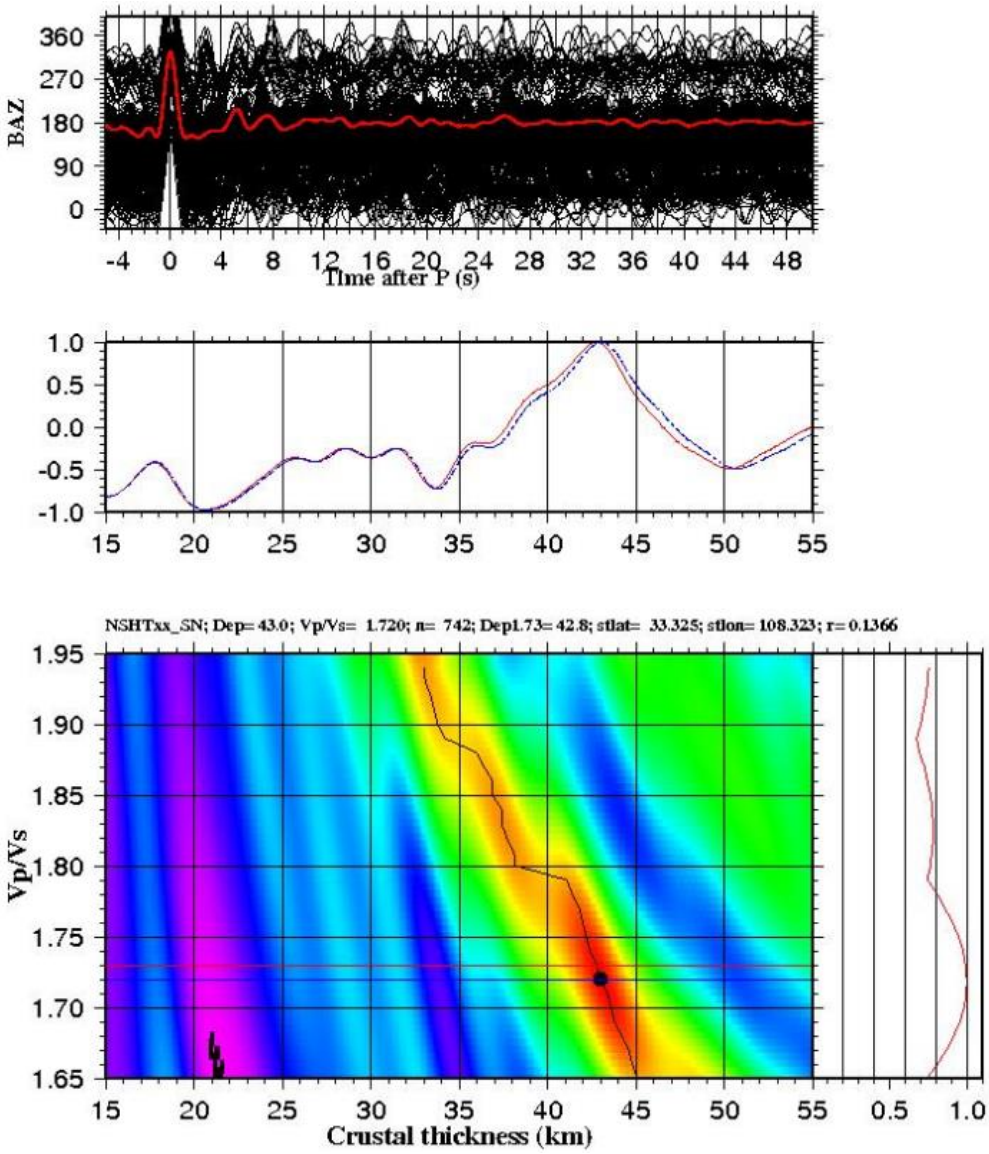

Figure S8. Example receiver function analyses for station NSHTxx_SN located in the Yangtze Platform. The dot represents the optimal H and Vp/Vs related to Moho.

APPENDIX B.

OBSERVATIONS OF EACH STATION

Table S1. Observations of Crustal Thickness (H) and Vp/Vs (Φ) of each station

Station Name	Lat*	Lon*	Ele*	H (km)	STD of H (km)	Φ	STD of Φ	N*	Area
AMUxxx_ZV	32.92	102.63	3500	48.99	0.20	1.778	0.004	168	B
ANKGxx_SN	32.67	109.04	392	50.07	0.07	1.852	0.004	855	A
ARWCxx_ZV	33.77	101.70	3511	54.87	0.46	1.745	0.013	97	B
ASTxxx_GZ	26.15	106.06	1342	35.47	0.05	1.730	0.000	202	D
AXIxxx_SC	31.64	104.43	611	41.53	0.14	1.748	0.004	757	D
AYUxxx_SC	30.05	105.34	366	41.99	0.28	1.816	0.008	197	D
BAMxxx_QH	32.95	100.73	3575	61.03	0.24	1.741	0.006	632	B
BAXxxx_SC	30.37	102.81	1214	44.72	0.69	1.778	0.013	198	D
BJTxxx_GZ	27.24	105.35	1472	46.86	0.07	1.731	0.003	585	D
BKTxxx_GS	32.79	105.71	669	40.86	0.24	1.847	0.007	306	D
BYDxxx_SC	27.81	103.19	3161	46.21	0.19	1.944	0.011	256	D
BZHxxx_SC	31.84	106.74	438	47.18	0.14	1.695	0.005	563	D
CD2xxx_CB	30.91	103.76	630	42.39	0.18	1.838	0.005	808	D
CHALxx_ZV	32.45	102.03	3721	50.91	0.12	1.761	0.003	167	B
CHKxxx_CQ	31.96	108.65	885	48.41	0.07	1.779	0.003	356	D
CHSxxx_CQ	29.91	107.23	354	40.23	0.25	1.855	0.009	685	D
CQTxxx_CQ	29.42	106.57	335	41.33	0.13	1.724	0.005	122	D
CUXxxx_YN	25.03	101.54	1835	46.66	0.13	1.708	0.004	728	C
CXIxxx_SC	31.71	105.95	424	42.48	0.33	1.695	0.021	86	D
CXTxxx_GS	33.73	105.76	1103	41.83	0.19	1.743	0.005	426	A
DALUxx_ZV	33.58	103.62	2849	47.25	0.13	1.819	0.003	198	B
DAWxxx_QH	34.48	100.25	3758	57.95	0.33	1.865	0.009	1018	A
DAYxxx_YN	25.73	101.32	1895	39.56	0.05	1.790	0.000	676	C
DBTxxx_GS	34.06	103.23	2495	40.61	0.19	1.843	0.007	779	B
DFUxxx_SC	30.99	101.12	3128	55.41	0.50	1.854	0.005	421	C
DJTxxx_GZ	28.22	108.13	800	40.72	0.11	1.667	0.007	300	D

EMSxxx_SC	29.58	103.45	486	48.78	0.13	1.748	0.004	549	D
ENHxxx_CD	30.28	109.50	450	46.20	0.00	1.820	0.000	1850	D
FULxxx_CQ	29.73	107.44	651	39.19	0.11	1.859	0.006	461	D
FUPIxx_SN	34.97	109.15	1157	32.63	0.23	1.903	0.012	222	A
GS02xx_X4	34.43	102.29	3433	51.71	0.14	1.793	0.005	246	A
GS05xx_X4	34.65	103.54	2781	47.87	0.17	1.774	0.005	238	A
GS07xx_X4	34.35	105.04	1844	42.10	0.00	1.750	0.000	291	A
GS10xx_X4	33.54	106.91	984	44.74	0.10	1.751	0.003	268	A
GS11xx_X4	33.91	105.97	1193	43.16	0.16	1.752	0.006	249	A
GS12xx_X4	34.85	105.75	1541	42.75	0.21	1.795	0.007	56	A
GYAxxx_CB	26.46	106.66	1125	39.29	0.03	1.701	0.003	1018	D
GZAxxx_SC	30.12	102.17	1719	55.94	0.21	1.904	0.008	995	C
GZIxxx_SC	31.61	100.02	3361	60.00	0.00	1.814	0.000	645	C
HEQxxx_YN	26.55	100.15	2281	50.52	0.21	1.783	0.005	598	C
HMSxxx_SC	29.57	104.40	742	44.49	0.26	1.806	0.007	857	D
HON2xx_ZV	34.06	102.45	3789	48.98	0.17	1.823	0.005	151	B
HSHxxx_SC	32.06	102.99	2506	52.36	0.14	1.751	0.003	571	B
HUAXxx_SN	34.40	109.72	864	32.37	0.20	1.770	0.009	704	A
HUHExx_ZV	34.90	100.90	3874	57.13	0.37	1.774	0.005	279	A
HUPxxx_YN	26.59	101.20	1298	51.08	1.43	1.823	0.046	632	C
HWSxxx_SC	28.64	104.74	640	39.87	0.21	1.785	0.007	717	D
HYSxxx_SC	30.42	106.84	528	42.26	0.08	1.779	0.003	744	D
HYUxxx_SC	32.81	102.52	3511	49.74	0.18	1.774	0.005	206	B
JJSxxx_SC	31.00	104.55	773	39.57	0.09	1.851	0.003	445	D
JLIxxx_SC	28.18	104.52	553	43.48	0.06	1.700	0.000	692	D
JLOxxx_SC	29.00	101.51	3136	58.14	0.38	1.858	0.011	681	C
JMGxxx_SC	32.21	105.56	847	41.26	0.05	1.780	0.000	596	D
JYAxxx_SC	29.79	103.93	534	47.38	0.26	1.873	0.007	669	D
JZGxxx_SC	33.26	104.24	1610	47.16	0.13	1.730	0.000	183	B
KMIxxx_CD	25.15	102.75	1985	42.90	0.00	1.800	0.000	3619	C

L0201x_OC	32.49	105.87	748	41.07	0.30	1.817	0.007	101	D
L0202x_OC	32.40	106.01	740	42.59	0.03	1.761	0.003	20	D
L0203x_OC	31.68	104.70	510	39.05	0.14	1.811	0.003	69	D
L0204x_OC	32.49	105.62	586	42.61	0.15	1.747	0.007	75	D
L0206x_OC	31.90	104.82	627	39.48	0.11	1.748	0.004	38	D
L0207x_OC	32.20	105.32	692	40.51	0.09	1.757	0.005	66	D
L0208x_OC	32.33	105.68	610	42.20	0.18	1.783	0.010	25	D
L0212x_OC	32.02	105.11	651	40.55	0.10	1.747	0.005	81	D
L0219x_OC	31.78	104.43	774	39.88	0.23	1.789	0.007	49	D
LANTxx_SN	34.11	109.38	727	34.05	0.16	1.778	0.006	128	A
LBTxxx_GZ	25.32	108.03	619	32.11	0.19	1.720	0.007	116	D
LCHxxx_HB	30.37	108.88	1300	42.96	0.23	1.851	0.006	876	D
LD5xxx_SN	33.04	108.24	421	47.10	0.38	1.819	0.009	104	A
LD6xxx_SN	32.61	107.15	969	46.86	0.30	1.722	0.009	116	D
LD7xxx_SN	33.91	106.52	1056	43.49	0.33	1.764	0.008	78	A
LDGxxx_HB	31.38	104.11	749	41.10	0.42	1.829	0.017	102	D
LDTxxx_GZ	25.43	106.75	490	34.30	0.00	1.720	0.000	388	D
LGHxxx_SC	27.71	100.86	2754	53.91	0.03	1.830	0.000	716	C
LIJxxx_YN	26.90	100.23	2473	52.54	0.25	1.839	0.006	222	C
LINTxx_SN	34.35	109.21	792	38.50	0.30	1.725	0.015	87	A
LIYOxx_SN	34.68	107.81	1082	44.34	0.10	1.743	0.005	682	A
LORIxx_ZV	32.49	102.44	3614	50.54	0.36	1.779	0.006	138	B
LOXTxx_SN	34.97	106.70	1490	46.12	0.15	1.787	0.005	857	A
LTAxxx_SC	30.00	100.27	3994	57.52	0.12	1.771	0.003	724	C
LTTxxx_GS	34.67	103.36	2806	46.00	0.00	1.790	0.000	684	A
LUQxxx_YN	25.54	102.45	1831	38.65	0.11	1.837	0.005	455	C
LUYAxx_SN	33.36	106.14	841	47.70	0.24	1.724	0.005	762	B
LZHxxx_SC	28.87	105.41	263	39.49	0.12	1.778	0.006	83	D
MALxxx_YN	25.43	103.58	2041	45.42	0.04	1.680	0.000	774	C
MAQUxx_ZV	34.02	102.06	3580	52.50	0.00	1.810	0.000	880	B

MBIxxx_SC	28.84	103.53	638	46.05	0.16	1.739	0.003	428	D
MC02xx_YA	30.62	103.22	1110	45.12	0.33	1.786	0.009	88	D
MC03xx_YA	30.00	102.49	1303	46.11	0.25	1.924	0.011	104	D
MC04xx_YA	30.06	101.48	3532	55.97	0.32	1.894	0.007	185	C
MC07xx_YA	29.05	100.42	3817	53.75	0.64	1.826	0.030	188	C
MDSxxx_SC	30.08	103.04	1142	40.84	0.13	1.963	0.007	194	D
MEIXxx_SN	34.13	107.82	972	40.02	0.09	1.769	0.006	749	A
MEKxxx_SC	31.90	102.22	2831	54.12	0.04	1.730	0.000	590	B
MGUxxx_SC	28.33	103.14	2087	50.10	0.00	1.840	0.000	493	D
MIAXxx_SN	33.23	106.80	1130	46.99	0.18	1.737	0.005	884	D
MNIxxx_SC	28.33	102.17	1662	55.39	0.17	1.893	0.005	536	C
MXIxxx_SC	31.68	103.85	1638	44.86	0.21	1.742	0.010	407	B
MXTxxx_GS	34.43	104.02	2329	45.02	0.17	1.742	0.004	874	A
NSHTxx_SN	33.33	108.32	949	43.14	0.14	1.717	0.005	742	A
PZHxxx_SC	26.47	101.74	1240	42.91	0.06	1.880	0.000	747	C
QCHxxx_SC	32.59	105.23	878	43.21	0.24	1.694	0.005	712	D
QIJxxx_CQ	29.56	108.80	999	42.50	0.00	1.810	0.000	547	D
QLITxx_SN	34.57	108.22	861	33.48	0.19	1.786	0.010	778	A
REGxxx_SC	33.58	102.97	3464	45.99	0.29	1.841	0.007	829	B
ROCxxx_CQ	29.38	105.44	435	38.86	0.13	1.771	0.003	757	D
RTAxxx_SC	32.27	100.98	3450	53.30	0.28	1.867	0.006	804	B
SHAZxx_SN	33.51	109.87	903	36.31	0.27	1.753	0.007	515	A
SHWAxx_SN	34.55	106.94	1102	42.13	0.21	1.777	0.005	312	A
SMIxxx_SC	29.23	102.35	1153	50.53	0.29	1.770	0.005	362	C
SMKxxx_SC	26.86	102.75	2292	54.33	0.25	1.807	0.006	217	C
SPAxxx_SC	32.65	103.60	2952	50.49	0.19	1.723	0.005	364	B
SRLNxx_ZV	34.48	102.14	3375	51.85	0.11	1.782	0.004	360	A
TABTxx_SN	34.07	107.29	1821	39.34	0.13	1.789	0.003	814	A
TANKxx_ZV	33.41	102.48	3434	51.54	0.55	1.718	0.011	8	B
TQUxxx_SC	30.07	102.76	816	43.94	0.21	1.889	0.004	154	D

TSSxxx_GS	34.34	106.02	1844	42.81	0.07	1.779	0.003	786	A
TUSxxx_YN	25.61	100.25	1969	42.66	0.14	1.765	0.005	397	C
WASxxx_CQ	28.88	106.92	596	41.96	0.07	1.701	0.003	823	D
WAZxxx_CQ	30.75	108.46	424	43.35	0.28	1.858	0.009	335	D
WCHxxx_SC	31.48	103.59	1438	51.39	0.22	1.878	0.004	692	B
WDTxxx_GS	33.36	104.99	1174	44.50	0.00	1.770	0.000	888	B
WMPxxx_SC	29.05	103.79	1148	39.68	0.19	1.886	0.005	952	D
WNTxxx_GZ	26.91	104.30	2335	42.37	0.13	1.696	0.005	253	D
WRCxxx_CQ	30.54	108.15	476	42.26	0.15	1.864	0.005	82	D
WSHxxx_GS	34.66	105.05	1742	41.73	0.05	1.740	0.000	629	A
WULxxx_CQ	29.19	107.83	400	41.16	0.12	1.750	0.000	374	D
WUXxxx_CQ	31.40	109.61	296	47.02	0.06	1.809	0.003	396	D
WXTxxx_GS	32.95	104.68	1093	46.80	0.11	1.680	0.000	851	B
XANxxx_IC	34.03	108.92	676	35.62	0.17	1.762	0.004	3655	A
XCOxxx_SC	31.02	105.90	348	43.50	0.00	1.800	0.000	611	D
XHAxxx_SC	31.37	107.72	376	46.90	0.26	1.766	0.007	582	D
XIXIxx_SN	32.91	107.72	602	44.63	0.17	1.820	0.007	766	D
XJIxxx_SC	31.00	102.35	2476	56.40	0.00	1.830	0.000	768	B
XUWxxx_YN	26.09	104.14	2140	45.92	0.12	1.700	0.000	744	D
YAJxxx_YN	28.11	104.23	682	42.90	0.08	1.779	0.003	690	D
YGDxxx_SC	30.20	104.10	687	40.07	0.05	1.888	0.003	501	D
YJIxxx_SC	30.03	101.01	2794	58.69	0.42	1.814	0.005	772	C
YOSxxx_YN	26.69	100.77	2253	53.99	0.16	1.730	0.000	461	C
YPTxxx_GZ	27.21	108.81	411	45.24	0.33	1.750	0.005	80	D
YUBxxx_CQ	29.86	106.83	336	39.10	0.00	1.820	0.000	754	D
YUMxxx_YN	25.69	101.86	1121	43.60	0.11	1.750	0.000	794	C
YYCxxx_SC	27.86	102.45	2772	55.37	0.11	1.869	0.003	1344	C
YYUxxx_SC	27.47	101.68	2612	57.75	0.14	1.838	0.004	496	C
YZPxxx_SC	30.87	103.57	757	41.53	0.09	1.844	0.005	324	D
ZATxxx_YN	27.32	103.72	1925	46.34	0.10	1.751	0.003	552	D

ZFTxxx_GZ	25.39	105.63	1122	34.01	0.03	1.769	0.003	216	D
ZHCxxx_GS	34.93	106.30	1848	43.74	0.14	1.752	0.004	554	A
ZHQxxx_GS	33.81	104.38	2094	41.27	0.09	1.851	0.003	245	A
ZJGxxx_SC	31.79	104.67	592	39.46	0.07	1.761	0.003	751	D
ZOZTxx_SN	34.06	108.32	664	39.40	0.00	1.711	0.000	935	A
ZUXxxx_HB	32.32	109.71	476	47.72	0.10	1.864	0.005	854	A
ZYTxxx_GZ	27.77	106.85	931	42.00	0.00	1.720	0.000	440	D

Lat* stands for the latitude in degree.

Lon* stands for the longitude in degree.

Elv* stands for the elevation in meter.

N* stands for the number of receiver functions used.

REFERENCES

Ammon, C.J. (1991). The isolation of receiver effects from te381 leseismic P waveforms, Bull. Seismo. Soc. Amer., 81, 2504-2510.

Bai, D., Unsworth, M.J., Meju, M.A., Ma, X., Teng, J., Kong, X., Sun, Y., Sun, J., Wang, L., Jiang, C., & Zhao, C. (2010). Crustal deformation of the eastern Tibetan plateau revealed by magnetotelluric imaging, Nature, 3, 358-362. http://doi: 10.1038/ngeo830

Balmino, G., Vales, N., Bonvalot, S., & Briais, A. (2012). Spherical harmonic modelling to ultra-high degree of Bouguer and isostatic anomalies, Journal of Geodesy, 86(7), 499-520

Bashir, L., Gao, S.S., Liu, K.H., & Mickus, K. (2011). Crustal structure and evolution beneath the Colorado Plateau and the southern Basin and Range Province: Results from receiver function and gravity studies, Geochem. Geophys. Geosys., 12, 1-6. http://doi: 10.1029/2011GC003563

Bonvalot, S., Balmino, G., Briais, A., Kuhn, M., Peyrefitte, A., & Vales, N. (2012). World Gravity Map, 1: 50000000 map, Eds: BGI-CGMW-CNES-IRD. Paris, 2012.http://bgi.obs-mip.fr/activities/Projects/world gravity map wgm

Bridges, D.L., Mickus, K., Gao, S.S., Abdelsalam, M.G., & Alemu, A. (2012). Magnetic stripes of a transitional continental rift in Afar, Geology, 40, 203-206. http://doi:10.1130/G32697.1

Budiansky, B., & O'connell, R.J. (1976). Elastic moduli of a cracked solid, International journal of Solids and Structures, 12, 81-97. http://doi: 10.1016/00207683(76)90044-5

Burchfiel, B. C., Zhiliang, C., Yupinc, L., & Royden, L. H. (402 1995). Tectonics of the Longmen Shan and adjacent regions, central China, International Geology Review, 37, 404 661-735

Christensen, N. I. (1996). Poisson's ratio and crustal seismology, J. Geophys. Res., 101, 3139-3156.

Clark, M.K. & Royden, L.H. (2000). Topographic ooze: Building the eastern margin of Tibet by lower crustal flow, Geology, 28,703-706. http://doi: 10.1130/00917613(2000)28 ¡703:TOBTEM ¿2.0.CO;2

Clayton, R.W., & Wiggins, R.A. (1976). Souce shape estimation and deconvolution of teleseismic bodywaves, Geophys. J. R. astr. Soc., 47, 151-177.

Deng, J.F., Mo, X.X., Zhao, H.E.A., Wu, Z.X., Luo, Z.H., & Su, S.G. (2004). A new model for the dynamic evolution of Chinese lithosphere:' continental roots-plume tectonics', Earth Sci. Rev., 65, 223-275. http://doi:10.1016/j.earscirev.2003.08.001

England, P., & Houseman, G. (1986). Finite strain calculations of continental deformation: 2. Comparison with the India-Asia collision zone, J. Geophys. Res., 91, 3664-3676. http://doi:10.1029/JB091iB03p03664

Feng, S.Y., Zhang, P.Z., Liu, B.J., Wang, M., Zhu, S.B., Ran, Y.K., Wang, W.T., Zhang, Z.Q., Zheng, W.J., Zheng, D.W., & Zhang, H.P. (2016). Deep crustal deformation of the Longmen Shan, eastern margin of the Tibetan Plateau, from seismic reflection, J. Geophys. Res., 121, 767-787. http://doi:10.1002/2015JB012352

Gan, W., Zhang, P., Shen, Z.K., Niu, Z., Wang, M., Wan, Y., Zhou, D., & Cheng, J. (2007). Present.day crustal motion within the Tibetan Plateau inferred from GPS measurements, J. Geophys. Res., 112. http://doi: 10.1029/2005JB004120

Gao, R., Wang, H., Zeng, L., Zhang, J., Guo, T., Li, Q., 425 Li, W., Li, P., & Guan, Y. (2014). The crust structures and the connection of the Songpan block and West Qinling orogen revealed by the Hezuo-Tangke deep seismic reflection profiling, Tectonophysics, 634, 227-236. http://doi:10.1016/j.tecto.2014.08.014

Gao, S. S., & Liu, K. H. (2014). Imaging mantle discontinuities using multiply-reflected P-to-S conversions, Earth Planet. Sci. Lett., 402, 99-106. http://doi:10.1016/j.epsl.2013.08.025

He, C., Dong, S., Santosh, M., & Chen, X. (2014). Seismic structure of the Longmenshan area in SW China inferred from receiver function analysis: Implications for future large earthquakes, Journal of Asian Earth Sciences, 96, 226-236. http://doi:10.1016/j.jseaes.2014.09.026

Hubbard, J., & Shaw, J.H. (2009). Uplift of the Longmen Shan and Tibetan plateau, and the 2008 Wenchuan (M= 7.9) earthquake, Nature, 458, 194-197. http://doi:10.1038/nature07837

Ji, S., Wang, Q., & Salisbury, M.H. (2009). Composition and tectonic evolution of the Chinese continental crust constrained by Poisson's ratio, Tectonophysics, 463, 15-30. http://doi:10.1016/j.tecto.2008.09.007

Jia, S., Zhang, X., Zhao, J., Wang, F., Zhang, C., Xu, Z., Pan, J., Liu, Z., Pan, S., & Sun, G. (2010). Deep seismic sounding data reveal the crustal structures beneath Zoige basin and its surrounding folded orogenic belts, Science China, 53, 203-212. http://doi:10.1007/s11430-009-0166-0

Jiang, W., Zhang, J., Tian, T., & Wang, X. (2012). Crustal structure of Chuan-Dian region derived from gravity data and its tectonic implications, Phys. Earth Planet. Inter., 212, 76-87. http://doi: 10.101448 6/j.pepi.2012.07.001

Kong, F., Wu, J., Liu, K.H., & Gao, S.S. (2016). Crustal anisotropy and ductile flow beneath the eastern Tibetan Plateau and adjacent areas, Earth Planet. Sci. Lett., 442, 72-79. http://doi: 10.1016/j.epsl.2016.03.003

Lei, J., & Zhao, D. (2009). Structural heterogeneity of the Longmenshan fault zone and the mechanism of the 2008 Wenchuan earthquake (Ms 8.0), Geochem. Geophys. Geosys., 10. http://doi: 10.1029/2009GC002590

Li, M., Zhang, S., Wang, F., Wu, T., & Qin, W. (2016). Crustal and upper-mantle structure of the southeastern Tibetan Plateau from joint analysis of surface wave dispersion and receiver functions, Journal of Asian Earth Sciences, 117, 52-63. http://doi: 10.1016/j.jseaes.2015.12.002

Li, X., Santosh, M., Cheng, S., Xu, X., & Zhong, W. (2015). Crustal structure and composition beneath the northeastern Tibetan Plateau from receiver function analysis, Phys. Earth Planet. Inter., 249, 51-58. http://doi: 10.1016/j.pepi.2015.10.001

Liu, M., Mooney, W.D., Li, S., Okaya, N., & Detweiler, S. (2006). Crustal structure of the northeastern margin of the Tibetan Plateau from the Songpan-Ganzi terrane to the Ordos basin, Tectonophysics, 420, 253-266. http://doi:10.1016/j.tecto.2006.01.025

Liu, Q.M., Zhao, J.M., Lu, F., & Liu H.B. (2014). Crustal structure of northeastern margin of the Tibetan Plateau by receiver function inversion, Science China, 57, 741-750. http://doi: 10.1007/s11430-013-4772-5

Liu, Q.Y., van der Hilst, R.D., Li, Y., Yao, H.J., Chen, J.H., Guo, B., Qi, S.H., Wang, J., Huang, H., & Li, S.C. (2014). Eastward expansion of the Tibetan Plateau by crustal flow and strain partitioning across faults, Nature, 7, 361-365. http://471 doi:10.1038/ngeo2130

Li, Y., Wang, X., Zhang, R., Wu, Q., & Ding, Z. (2017). Crustal structure across the NE Tibetan Plateau and Ordos Block from the joint inversion of receiver functions and Rayleigh-wave dispersions, Tectonophysics, 705, 33-41. http://doi:10.1016/j.tecto.2017.03.020

Lou, H., Wang, C., L, Z., Yao, Z., Dai, S., & You, H. (2009). Deep tectonic setting of the 2008 Wenchuan Ms 8.0 earthquake in southwestern China. Science, 52, 166-179. http://doi:10.1007/s11430-009-0009-z

Meng, W., Yan-ming, Z., Guo-qiang, W., & Wen-yong, Z. (2009). Oil-gas characteristics controlled by coalifications in upper triassic sedimentary organic matters in Chuxiong basin, Procedia Earth and Planetary Science, 1, 1002-1009. http://doi:10.1016/j.proeps.2009.09.155

Nair, S.K., Gao, S.S., Liu, K.H., & Silver, P.G. (2006). Southern African crustal evolution and composition: Constraints from receiver function studies, J. Geophys. Res., 111, B02304. http://doi:101029/2005JB003802

Owens, T.J., & Zandt, G. (1997). Implications of crustal property variations for models of Tibetan plateau evolution, Nature, 387, 37-43. http://doi:10.1038/387037a0

Pei, S., Zhang, H., Su, J., & Cui, Z. (2014). Ductile gap between the Wenchuan and Lushan earthquakes revealed from the two-dimensional Pg seismic tomography, Scientific reports, 4, 6489. http://doi:10.1038/srep06489

Qian, Q., & Hermann, J. (2013). Partial melting of lower crust at 10-15 kbar: constraints on adakite and TTG formation, Contributions to Mineralogy and Petrology, 165, 1195-1224. http://doi:10.1007/s00410-013-0854-9

Reed, C.A., Almadani, S., Gao, S.S., Elsheikh, A.A., Cherie494 , S., Abdelsalam, M.G., Thurmond, A.K., & Liu, K.H. (2014). Receiver function constraints on crustal seismic velocities and partial melting beneath the Red Sea rift and adjacent regions, Afar Depression, J. Geophys. Res., 119, 2138-2152. http://doi:10.1002/2013JB010719

Robert, A., Zhu, J., Vergne, J., Cattin, R., Chan, L. S., Wittlinger, G., Herquel, G., De Sigoyer, J., Pubellier, M., & Zhu, L. D. (2010). Crustal structures in the area of the 2008 Sichuan earthquake from seismologic and gravimetric data, Tectonophysics, 491, 205-210. http://doi:10.1016/j.tecto.2009.11.010

Roydenn, L.H., Burchfiel, B.C., King, R.W., Wang, E., Chen, Z., Shen, F., & Liu, Y. (1997). Surface deformation and lower crustal flow in eastern Tibet, Science, 276, 788-790. http://doi:10.1126/science.276.5313.788

Royden, L.H., Burchfiel, B.C., & van der Hilst, R.D. (2008). The geological evolution of the Tibetan Plateau, Science, 321, 1054-1058. http://doi:10.1126/science.1155371

Shen, Z.K., Lu, J., Wang, M., & Burgmann, R. (2005). Contemporary crustal deformation around the southeast borderland of the Tibetan Plateau, J. Geophys. Res., 110, B11. http://doi:10.1029/2004JB003421

Sun, Y., Liu, J., Zhou, K., Chen, B., & Guo, R. (2015). Crustal structure and deformation under the Longmenshan and its surroundings revealed by receiver function data, Phys. Earth Planet. Inter., 244, 11-22. http://doi:10.1016/j.pepi.2015.04.005

Tarkov, A.P., & Vavakin, V.V. (1982). Poisson's ratio behaviour in various crystalline rocks: application to the study of the Earth's interior, Phys. Earth Planet. Inter., 29, 24-29. http://doi:10.1016/0031-9201(82)90134-0

Tapponnier, P., Zhiqin, X., Roger, F., Meyer, B., Arnaud, N., Wit517 tlinger, G., & Jingsui, Y. (2001). Oblique stepwise rise and growth of the Tibet Plateau, Science, 294, 1671-1677. http://doi:10.1126/science.105978

Wang, C.Y., Han, W.B., Wu, J.P., Lou, H., & Chan, W.W. (2007). Crustal structure beneath the eastern margin of the Tibetan Plateau and its tectonic implications, J. Geophys. Res., 112, B7. http://doi:10.1029/2005JB003873

Wang, C.Y., Zhu, L., Lou, H., Huang, B.S., Yao, Z., & Luo, X. (2010). Crustal thicknesses and Poisson's ratios in the eastern Tibetan Plateau and their tectonic implications, J. Geophys. Res., 115, B11. http://doi:10.1029/2010JB007527

Wang, E., Kirby, E., Furlong, K.P., Van Soest, M., Xu, G., Shi, X., Kamp, P.J., & Hodges, K.V. (2012). Two-phase growth of high topography in eastern Tibet during the Cenozoic, Nature, 5, 640-645. http://doi:10.1038/ngeo1538

Wang, Y., Mooney, W.D., Yuan, X., & Okaya, N. (2013). Crustal structure of the northeastern Tibetan Plateau from the southern Tarim Basin to the Sichuan Basin, China, Tectonophysics, 584, 191-208. http://doi:10.1016/j.tecto.2012.09.003

Wang, Z., Wang, J., Chen, Z., Liu, Y., Huang, R., Pei, S., Zhang, Q., & Tang, W. (2011). Seismic imaging, crustal stress and GPS data analyses: Implications for the generation of the 2008 Wenchuan Earthquake (M7.9), China, Gondwana Research, 19, 202-212. http://doi:10.1016/j.gr.2010.05.004

Wu, Y., Gao, S., Zhang, H., Zheng, J., Liu, X., Wang, H., Gong, H., Zhou, L., & Yuan, H. (2012). Geochemistry and zircon U-Pb geochronology of Paleoproterozoic arc related granitoid in the Northwestern Yangtze Block and its geological implications, Precambrian Research, 200, 26-37.

Xiong, X., Gao, R., Zhang, J., Wang, H., & Guo, L. (2015). Diff erences of Structure in Mid-Lower Crust between the Eastern and Western Blocks of the Sichuan basin, Chinese Journal of Geophysics, 58, 363-374. http://doi:10.1002/cjg2.20180

Xiong, X., Gao, R., Wang, H., Zhang, J., & Guo, L. (2016). Frozen subduction in the Yangtze block: insights from the deep seismic profiling and gravity anomaly in east Sichuan fold belt, Earthq. Sci., 29, 61-70. http://doi:10.1007/s11589-016-0140-9

Xu, L., Rondenay, S., & van der Hilst, R.D. (2007). Structure of the crust beneath the southeastern Tibetan Plateau from teleseismic receiver functions, Phys. Earth Planet. Inter., 165, 176-193. http://doi:10.1016/j.pepi.2007.09.002

Xu, X., Ding, Z., Shi, D., & Li, X. (2013). Receiver function analysis of crustal structure beneath the eastern Tibetan plateau, Journal of Asian Earth Sciences, 73, 121-127. http://doi:10.1016/j.jseaes.2013.04.018

Xu, X., Gao, R., & Guo, X. (2016). Relationship between the regional tectonic activity and crustal structure in the eastern Tibetan plateau discovered by gravity anomaly, Earthquake Science, 29, 71-81. http://doi:10.1007/s11589-016-0142-7

Xu, X., Wen, X., Chen, G., & Yu, G. (2008). Discovery of the Longriba fault zone in eastern Bayan Har block, China and its tectonic implication, Science in China, 51, 1209-1223. http://doi:10.1007/s11430-008-0097-1

Yin, A., & Harrison, T.M. (2000). Geologic evolution of the Himalayan-Tibetan orogen, Ann. Rev. Earth Planet. Sci., 28, 211-280. http://doi:10.1146/annurev.earth.28.1.211

Yin, A., & Nie, S. (1993). An indentation model for the North and South China collision and the development of the Tan.Lu and Honam fault systems, eastern Asia, Tectonics, 12, 801-813. http://doi:10.1029/93TC00313

Zhang, J., Gao, R., Zeng, L., Li, Q., Guan, Y., He, R., W563 ang, H., & Lu, Z. (2010). Relationship between characteristics of gravity and magnetic anomalies and the earthquakes in the Longmenshan range and adjacent areas, Tectonophysics, 491(1-4), pp.218-229.

Zhang, Z., Yuan, X., Chen, Y., Tian, X., Kind, R., Li, X., & Teng, J. (2010). Seismic signature of the collision between the east Tibetan escape flow and the Sichuan Basin, Earth Planet. Sci. Lett., 292, 254-264. http://doi:10.1016/j.epsl.2010.01.046

Zhang, Y., Teng, J., Wang, Q., & Hu, G. (2014). Density structure and isostatic state of the crust in the Longmenshan and adjacent areas, Tectonophysics, 619, 51-57. http://doi:10.1016/j.tecto.2013.08.018

Zhao, G. & Cawood, P.A., (2012). Precambrian geology of China, Precambrian Research, 222, pp.13-54.

Zhao, G., Unsworth, M.J., Zhan, Y., Wang, L., Chen, X., Jones, A.G., Tang, J., Xiao, Q., Wang, J., Cai, J., & Li, T. (2015). Crustal structure and rheology of the Longmenshan and Wenchuan Mw 7.9 earthquake epicentral area from magnetotelluric data, Geology, 40, 1139-1142. http://doi:10.1130/G33703.1

VITA

Yunxin Peng received her bachelor degree in Geophysics from Chengdu University of Technology in China in 2012. She worked in oversea marketing with IObit in Chengdu after obtained her B.S. degree.

In 2013, Yunxin joined Missouri University of Science and Technology to pursue PhD degree in geology and geophysics. Her research interests involved studying crustal structure using receiver functions analysis and crustal and mantle attenuation of seismic body-wave using spectral ratio method. During her studying in the Missouri S&T, she was also an associate graduate research assistant with Tongji University (China) focusing on seismic processing and interpretation. In summer 2017, she interned in Agricultural Bank of China for two months in Shanghai. Later that year, she was honored Thomas Beveridge Outstanding Graduate Teaching Assistant Award for being an outstanding teaching assistant of seismic interpretation class and elastic wave theory class in MST. Besides the communication and teaching skills, Yunxin developed some technical skills after entered Missouti S&T including 2D and 3D seismic processing and interpretation (Petrel, Kingdom, Hampson-Russel, and Landmark 5000), programming (FORTRAN, C Language, and Python), geographic information system (GMT, CorealDraw, Capaware, and Google Earth Digitization). In July 2018, she received her PhD in Geology and Geophysics from Missouri S&T.